Syn-thinning pluton emplacement during Mesozoic extension in eastern Mongolia

Yannick Daoudene, Denis Gapais, Gilles Ruffet, Eric Gloaguen, Alain Cocherie, Patrick Ledru

Syn-thinning pluton emplacement during Mesozoic extension in eastern Mongolia

Yannick Daoudene,[1,2] Denis Gapais,[1,2] Gilles Ruffet,[1,2] Eric Gloaguen,[3] Alain Cocherie,[3] and Patrick Ledru[3,4]

Received 18 April 2011; revised 1 March 2012; accepted 6 March 2012; published 4 May 2012.

[1] This paper documents relationships between deformation and magmatic activity that occurred in the central part of eastern Mongolia during late Mesozoic continental-scale NW-SE extension. Two coarse-grained, biotite-bearing, syn-tectonic intrusions are described. The Nartyn granite that extends over an area greater than 30 by 10 km was emplaced within low-grade metasediments and shows a weak pervasive, magmatic fabric reworked by solid-state deformation along its margins. The northwestern roof of the granite is marked by a normal shear zone, the Choyr Shear Zone, characterized by top-to-the-NW motions. The shear zone is overlain by the Choyr Basin, which is filled with unmetamorphosed continental sedimentary rocks of early Cretaceous ages. From structural and geochronological data, we propose that the Nartyn massif was emplaced as a flat laccolith-type intrusion at ca. 136–130 Ma during crustal thinning. The Altanshiree granite, located ~140 km east of the Nartyn granite, is a syn-kinematic pluton of similar age (134–128 Ma), also emplaced during crustal thinning. In the Nartyn and Altanshiree areas, extension implies pervasive crustal thinning, combined with limited exhumation. These areas are different from classical metamorphic core complexes, where strong strain localization along detachments induces exhumation of hot middle to lower crust. Results also suggest that early Cretaceous syn-extensional intrusions are an important feature of the tectonic history of eastern Mongolia.

Citation: Daoudene, Y., D. Gapais, G. Ruffet, E. Gloaguen, A. Cocherie, and P. Ledru (2012), Syn-thinning pluton emplacement during Mesozoic extension in eastern Mongolia, *Tectonics*, *31*, TC3001, doi:10.1029/2011TC002926.

1. Introduction

[2] The geological architecture of Mongolia is commonly interpreted as a result of a long period of north-south convergence, leading to the formation of one of the largest accretionary complexes on the Earth, the Central Asian Fold/Orogenic Belt [*Zonenshain et al.*, 1990; *Mossakovsky et al.*, 1993; *Badarch et al.*, 2002], also known as the Altaids [*Suess*, 1908; *Şengör et al.*, 1993; *Şengör and Natal'in*, 1996; *Yakubchuk et al.*, 2001]. This belt lies between the Siberian Craton to the North and the Sino-Korean and Tarim Cratons to the South, and extends from the Urals in the West to the Sikhote-Alin Range in the Russian Far East [e.g., *de Jong et al.*, 2009]. The formation of the Central Asian Orogenic Belt lasted ca. 750 Ma, beginning in Transbaikalia during Neoproterozoic times [*Khain et al.*, 2002] and finishing in northern China during the early Permian [*Hsü et al.*, 1991; *Şengör and Natal'in*, 1996, *Xiao et al.*, 2003] or Permian to early Triassic times [*Chen et al.*, 2009].

[3] During the last decades, numerous studies focused on a large-scale NW-SE extension that occurred during late Jurassic to early Cretaceous times throughout eastern Asia [*Zorin*, 1999; *Ren et al.*, 2002; *Meng*, 2003; *Darby et al.*, 2004; *Lin and Wang*, 2006]. This major tectonic event that extends from Transbaikalia in Russia to northeastern China is marked by (1) the widespread occurrence of continental sedimentary basins [*Watson et al.*, 1987; *Traynor and Sladen*, 1995; *Allen et al.*, 1998; *Khand et al.*, 2000; *Ren et al.*, 2002; *Meng et al.*, 2003] described as NE-SW trending rift basins [e.g., *Meng*, 2003; *Meng et al.*, 2003] (Figure 1) and mainly filled with late Jurassic to early Cretaceous sediments and volcanics [e.g., *Graham et al.*, 2001], and (2) metamorphic core complexes documented in Transbaikalia-northern Mongolia and northeastern China [*Sklyarov et al.*, 1994, 1997; *Davis et al.*, 1996, 2002; *Webb et al.*, 1999; *Darby et al.*, 2004; *Liu et al.*, 2005; *Mazukabzov et al.*, 2006; *Donskaya et al.*, 2008; *Daoudene et al.*, 2009; *Charles et al.*, 2011] (Figure 1). Geochronological studies point to core complex development during early Cretaceous times [*Sklyarov et al.*, 1997; *Donskaya et al.*, 2008; *Webb et al.*, 1999; *Davis et al.*, 2002; *Zhang et al.*, 2002, 2003; *Lin et al.*, 2008], with a likely peak of exhumation in a narrow time range between 130 Ma and 125 Ma [*Daoudene et al.*, 2011].

[1]CNRS (CNRS/INSU) UMR 6118, Géosciences Rennes, Rennes, France.
[2]Géosciences Rennes, Université de Rennes 1, Rennes, France.
[3]BRGM, Orléans, France.
[4]Now at AREVA, KATCO, Almaty, Kazakhstan.

0278-7407/12/2011TC002926

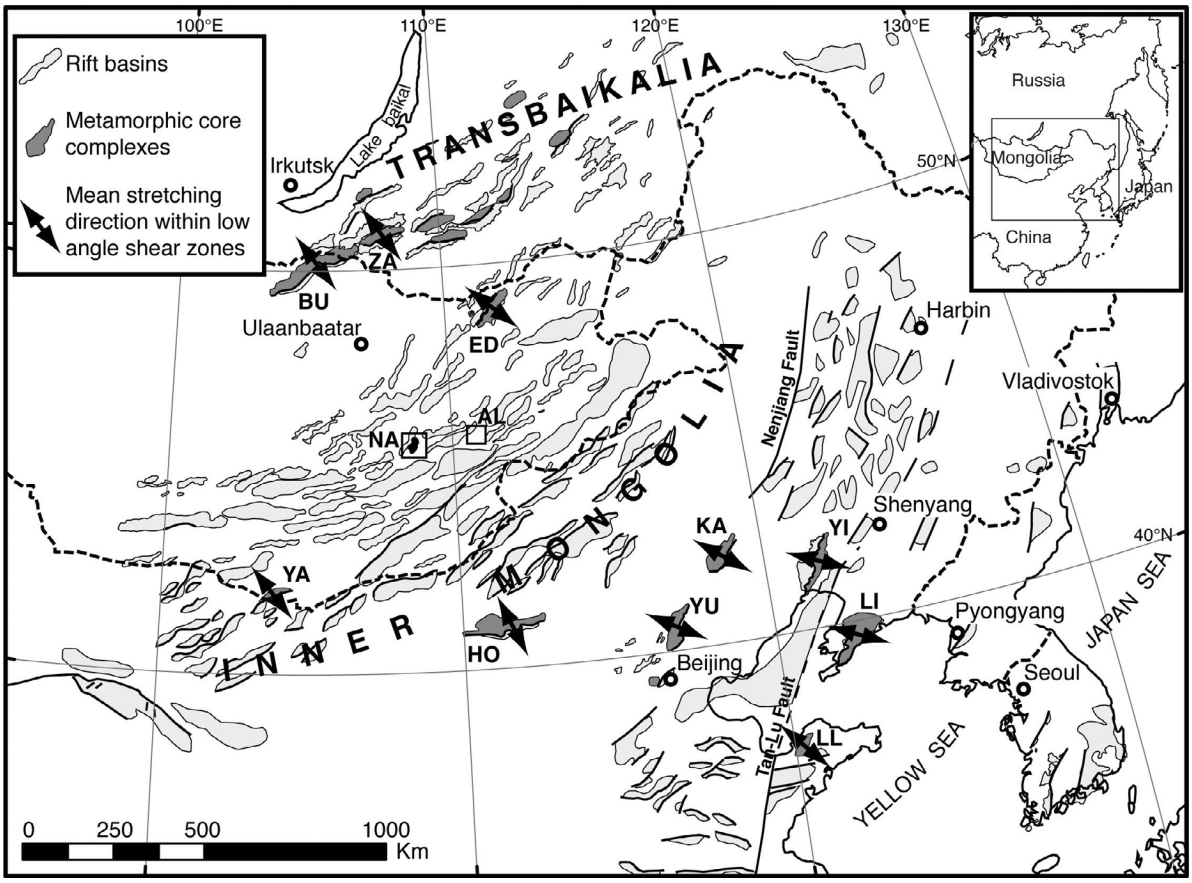

Figure 1. Late Jurassic to early Cretaceous extensional structures in the eastern part of the Asian Continent [modified after *Daoudene et al.*, 2009]. Localization of rifts basins is after *Zorin* [1999], *Ren et al.* [2002], and *Meng* [2003]. Metamorphic core complexes: BU, Buteel-Burgutoy [*Mazukabzov et al.*, 2006; *Donskaya et al.*, 2008]; ED, Ereendavaa [*Daoudene et al.*, 2009, 2011]; HO, Hohhot [*Davis et al.*, 2002]; KA, Kalaqin [*Zhang et al.*, 2003]; LI, Liaoning [*Liu et al.*, 2005]; LL, Linglong [*Charles et al.*, 2011]; Transbaikalia [*Zorin*, 1999; *Mazukabzov et al.*, 2006; *Donskaya et al.*, 2008]; YA, Yagan-Onch Hayrhan [*Webb et al.*, 1999]; YI, Yiwulüshan [*Zhang et al.*, 2003; *Darby et al.*, 2004]; YU, Yunmengshan [*Davis et al.*, 1996]; ZA, Zagan [*Sklyarov et al.*, 1994, 1997; *Donskaya et al.*, 2008]. NA and AL Nartyn and Altanshiree areas studied in this paper.

[4] The entire region was marked by widespread magmatic activity since 170–160 Ma [*Yarmolyuk et al.*, 1998; *Yarmolyuk and Kovalenko*, 2001; *Kovalenko et al.*, 2004; *Jahn et al.*, 2009]. Compilations of geochronological data suggest that magmatic activity reached a peak between 130 Ma and 120 Ma [e.g., *Wu et al.*, 2005; *Wang et al.*, 2006] coeval with the exhumation of several metamorphic core complexes.

[5] This paper presents new structural and U-Pb and $^{40}Ar/^{39}Ar$ geochronological data on the Nartyn granitic massif. The massif is bounded to the northwest by the Choyr Shear Zone, a recently recognized normal shear zone [*Daoudene et al.*, 2009], that shows comparable geometry and orientation as detachments associated with metamorphic core complexes in the region. However, in contrast to classic metamorphic core complexes, rocks exhumed in the footwall show limited metamorphic conditions. These features lead us to examine the age and emplacement dynamics of the Massif. The tectonic interpretation of the Nartyn massif is further supported by additional observations and geochronological analyses made in the Altanshiree area, ~140 km farther east.

2. Lithologies of the Nartyn Area

[6] The Nartyn massif is located in the central part of eastern Mongolia about 270 km southeast of Ulaanbaatar (Figure 1). The massif is bounded to the northwest by the NE-SW trending Choyr Basin (Figure 2a) that is a part of a large basin domain in the central part of eastern Mongolia, the Choyr-Nyalga Basin [e.g., *Erdenetsogt et al.*, 2009]. The basin is filled with unmetamorphosed, non-lithified continental sediments with a total thickness of about 1500 m [*Gow and Pool*, 2007]. The sedimentary pile comprises alternating conglomerates and sandstone, overlain by sandstones, mudstones and shales [e.g., *Ito et al.*, 2006; *Nichols et al.*, 2006; *Saiki and Okubo*, 2006; *Sha et al.*, 2006]. The age of sediments was initially considered to range between ~155 Ma and ~125 Ma [*Matsukawa et al.*, 1997]. More recent studies, based on magnetostratigraphy [*Hicks et al.*, 1999] and

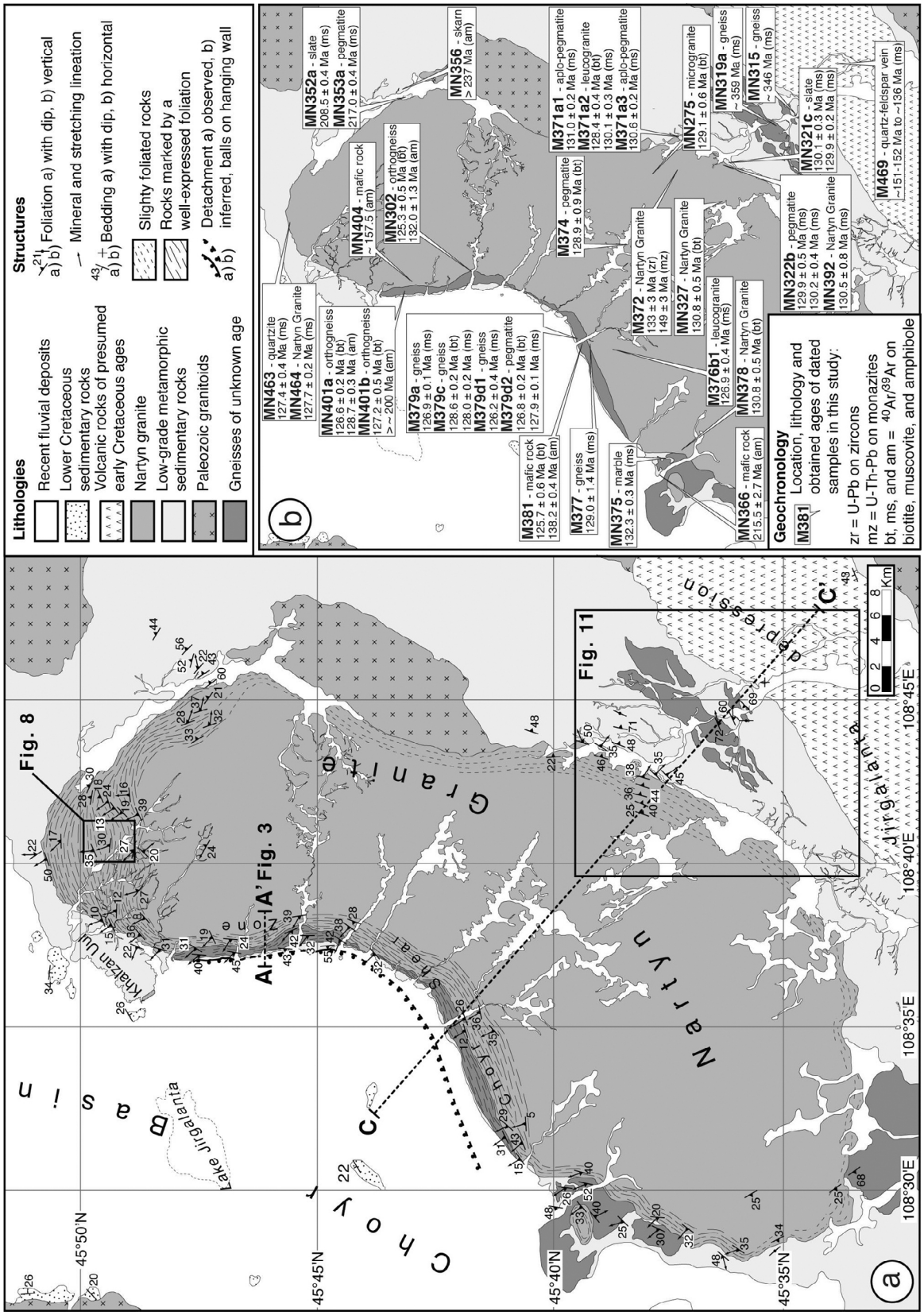

Figure 2. (a) Simplified geological map of the Nartyn massif (from personal field observations and interpretations of Google Earth satellite images). Location in Figure 1. (b) Map of the Nartyn massif with locations of samples used for geochronological analyses. U-Pb zircon and U-Th-Pb monazite age errors are at 2σ levels. All $^{40}Ar/^{39}Ar$ age errors are given at the 1σ level.

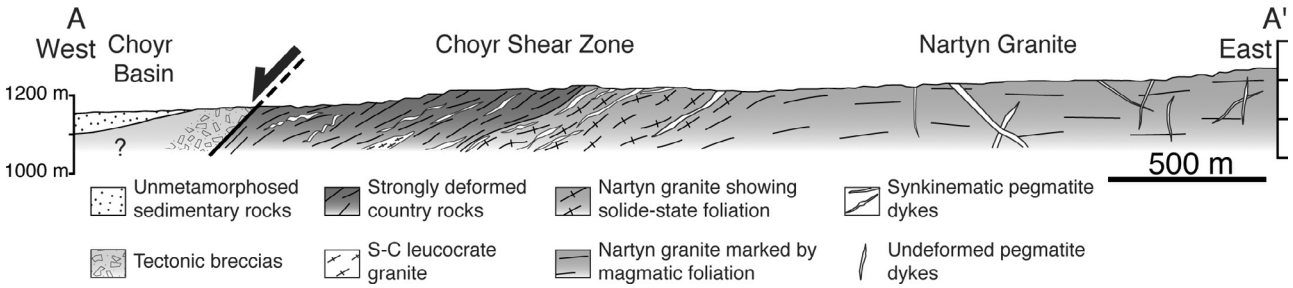

Figure 3. Simplified WE cross-section across the northwestern border of the Nartyn massif. Location on Figure 2a. The interface between the Nartyn massif and the overlying Choyr Basin is a normal shear zone, the Choyr Shear Zone.

palynology [*Nichols et al.*, 2006] indicate that the youngest deposits might be ~100 Ma in age. The lower Cretaceous sediments are overlain by a 5 to 40 m-thick deposit of upper Cretaceous sand and gravel [*Gow and Pool*, 2007]. The interface between the Choyr Basin and the Nartyn massif was previously mapped as a complex of high angle normal and/or strike-slip faults [*Yanshin*, 1989; *Matsukawa et al.*, 1997]. *Daoudene et al.* [2009] have recently proposed that it might be a low-angle normal shear zone.

[7] The Nartyn massif is an elongate NE-SW trending granitic intrusion extending over an area of 30 by 10 km. Country rocks are mainly metasediments (Figure 2a) comprising dark blue quartzite, slate, and grayish-laminated marble containing archeocyathes and stromatolites, considered as Neoproterozoic to Cambrian in age [*Amantov*, 1966; *Byamba et al.*, 1990, *Badarch et al.*, 2002]. Close to the granite contact, numerous dykes of leucogranite, pegmatite and aplite intrude the country rocks. The metasediments overlie a crystalline basement made of gneisses, amphibolites and granitoids that are crosscut by numerous mafic dykes.

[8] The core of the Nartyn intrusion is a coarse-grained biotite granite, which presents irregular accumulations of feldspar phenocrysts and rare microgranular enclaves. Along its boundaries, the granite shows finer grain sizes with frequent occurrence of muscovite. Pegmatitic and microgranitic dykes are widespread throughout the intrusion. Along its margins, and especially close to the northern edge, the granite contains large xenoliths and panels of country rocks, including coarse-grained marble, slate, but also other lithologies such as amphibolite and migmatitic gneisses that were not recognized within the adjacent country rocks.

3. Structure

3.1. The Choyr Shear Zone

[9] At the northwestern edge of the Nartyn granite, the Choyr Shear Zone comprises foliated metamorphic and magmatic rocks (Figure 3). Rocks show a well-expressed NE-SW to NS striking foliation that roughly follows the border of the granite (Figure 2a). The foliation dips shallowly (~20–45°) toward the Choyr Basin. Foliation planes bear a well-defined NW-SE trending mineral and stretching lineation marked by the preferred orientation of biotite, amphibole, and quartz-feldspar aggregates. Shear sense indicators are widespread, including S-C fabric and shear bands (Figure 4a), rolling structures (Figure 4b), and asymmetric boudins of pegmatite dykes (Figure 4c). All shear sense indicators attest to top-to-the-NW motions.

[10] Toward the Choyr Basin, within the uppermost levels of the shear zone, deformation is represented by brittle structures. Normal faults cut across rocks that were previously deformed under ductile conditions (Figure 4d) and bands of cataclasite up to 20 m thick are locally observed (Figure 5). These brecciated zones dip toward the basin and their attitude, together with the downdip striae that mark west-dipping fault surfaces, appear consistent with that of the underlying ductile fabrics. Above the main band of cataclasites, scarce outcrops of brecciated marble tend to show a decreasing amount of brittle deformation toward the Choyr Basin. These marble units belong probably to the base of the hanging wall of the shear zone.

3.2. The Nartyn Intrusion

3.2.1. Granite Core

[11] In most places, the core of the intrusion shows a macroscopic flat-lying fabric (Figure 6a). Euhedral feldspar phenocrysts form local irregular accumulations and, where abundant, they frequently show imbrications, a feature suggesting grain rotation and tiling in a viscous fluid [e.g., *Blumenfel*, 1983; *Paterson et al.*, 1989]. Nevertheless, the granite does not show mineral preferred orientation or internal grain deformation (Figure 6b), which demonstrates that the magmatic fabric is poorly expressed at the grain scale and suggests a lack of sub-solidus deformation.

3.2.2. Granite Margin

[12] The margins of the granite exhibit solid-state deformation marked by a foliation sub-parallel to the contact with country rocks, gently dipping away from the core of the intrusion (Figure 2a). The foliation is well developed along the northwestern margin where it bears a NW-SE directed stretching lineation (Figures 2a and 7a). It is much weaker along the southeastern margin, with a weak or absent stretching lineation. Scarce, discrete shear bands attesting to top-to-the-NW motions are observed along the northern margin of the intrusion (Figure 7b).

[13] Deformation is associated with extensive grain size reduction (Figure 7c). Quartz and feldspar display undulatory extinctions. K-feldspar shows evidence of extensive dynamic recrystallization with fine-grained mantles surrounding remnants of old large grains (Figure 7c), which suggests T > 550°C [e.g., *Pryer*, 1993]. Myrmekite occurs along K-feldspar faces that are sub-parallel to the foliation (Figure 7c), also

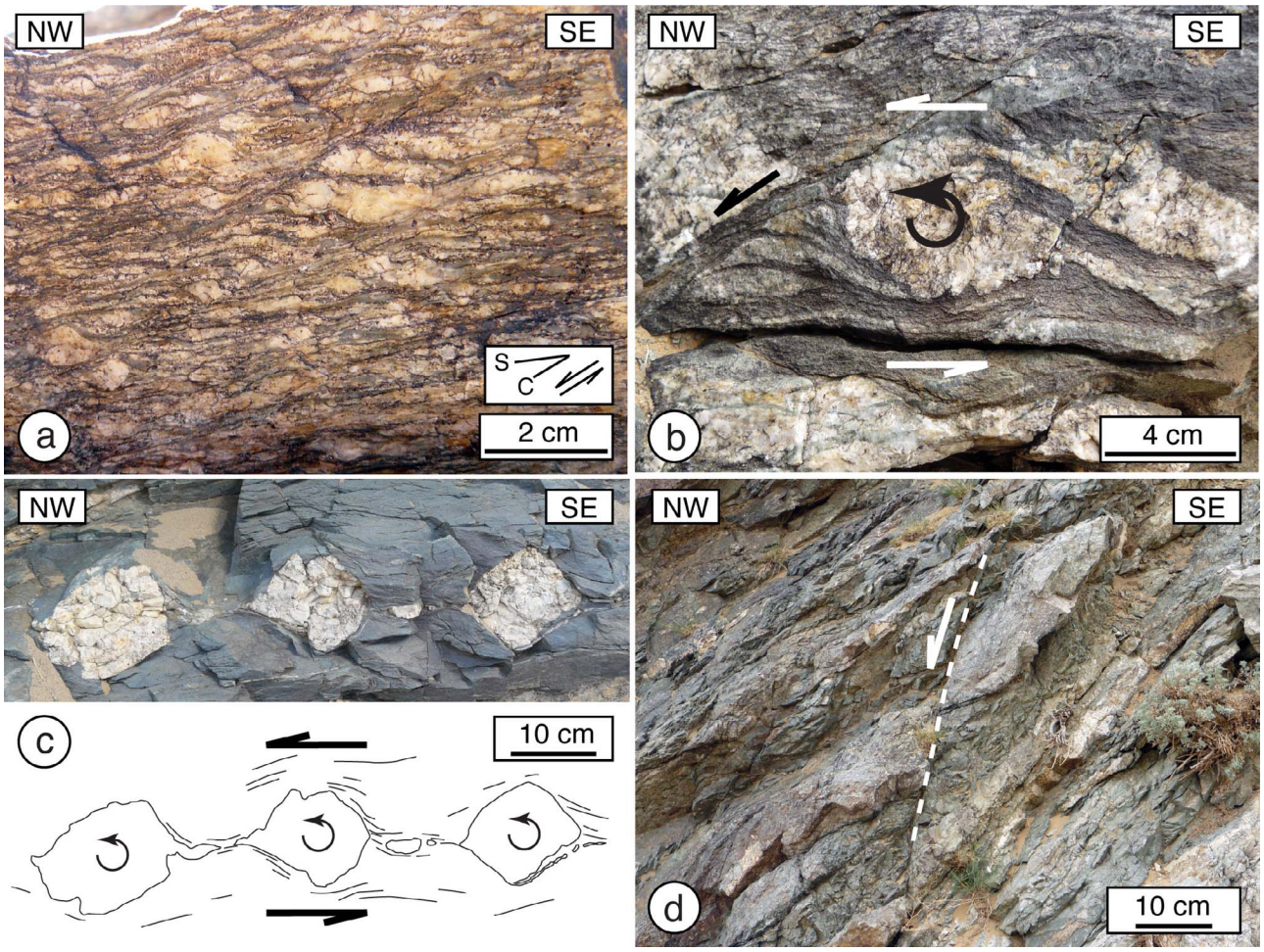

Figure 4. Photographs and interpretative line-drawings of top-to-the-NW kinematic indicators in the Choyr Shear Zone (view perpendicular to foliation and parallel to lineation). (a) Felsic orthogneiss with association of pervasive foliation (S) and ductile shear bands (C). (b) Rolling structure in paragneisses. (c) Asymmetric boudinage of a pegmatite dyke parallel to foliation of the host rock. (d) Normal microfault affecting series of strongly foliated orthogneisses.

indicating temperatures of ~550°C or more during deformation [*Simpson*, 1985; *Simpson and Wintsch*, 1989]. Core-and-mantle structures and myrmekite around K-feldspar phenocrysts are more frequent along the southeastern edge of the Nartyn intrusion. Chessboard-type structures may be observed within quartz grains along the southeastern margins of the Nartyn intrusion (Figure 7d), which attest to combined intracrystalline slip along < a > and < c > directions and indicate deformation under sub-solidus thermal conditions higher than ~600°C [*Blumenfeld et al.*, 1986; *Gapais and Barbarin*, 1986; *Mainprice et al.*, 1986; *Schmid and Casey*, 1986; *Stipp et al.*, 2002]. Extensive grain size reduction at the granite boundary suggests that the HT deformation was followed by a retrograde stage.

3.2.3. Xenoliths and Country Rocks Sheets

[14] Xenoliths and sheets of country rocks are observed along the northern margin of the Nartyn intrusion (Figure 8a). At the vicinity of the contact, they consist of country rocks directly adjacent to the intrusion (i.e., marble, quartzite and slate). Marble shows extensive annealing marked by large grain size. The granite also contains sheets and xenoliths of layered amphibolite (Figure 9a) with alternating pyroxene-rich

Figure 5. Cataclastic granitoid from the uppermost part of the Choyr Shear Zone.

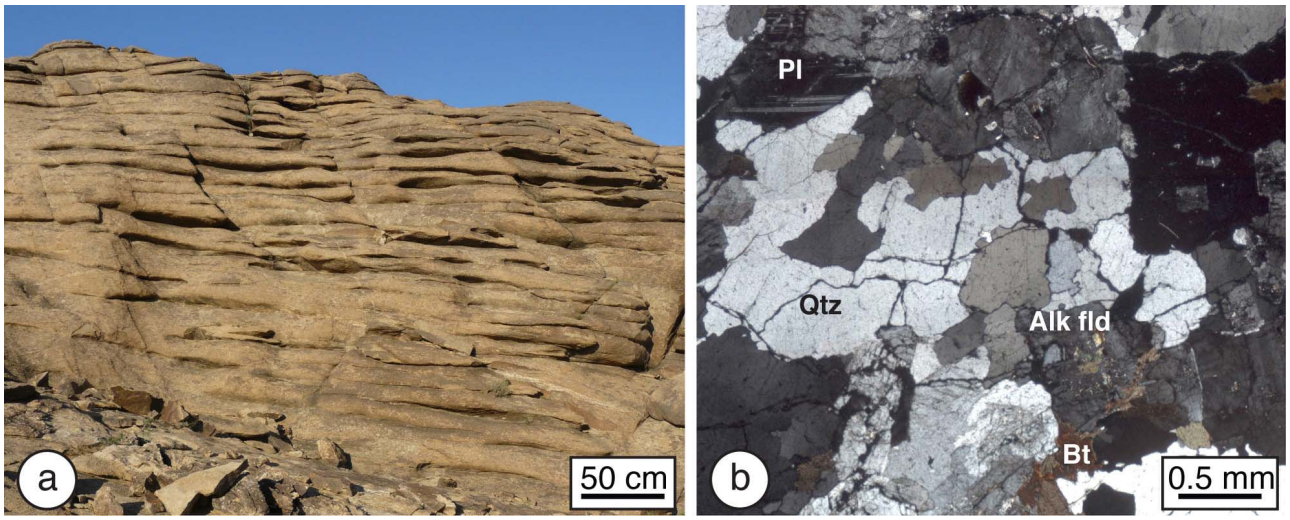

Figure 6. (a) Homogeneous porphyritic granite in the core of the Nartyn intrusion. The granite is marked by a pervasive flat-lying fabric. (b) Thin section in cross-polarized light.

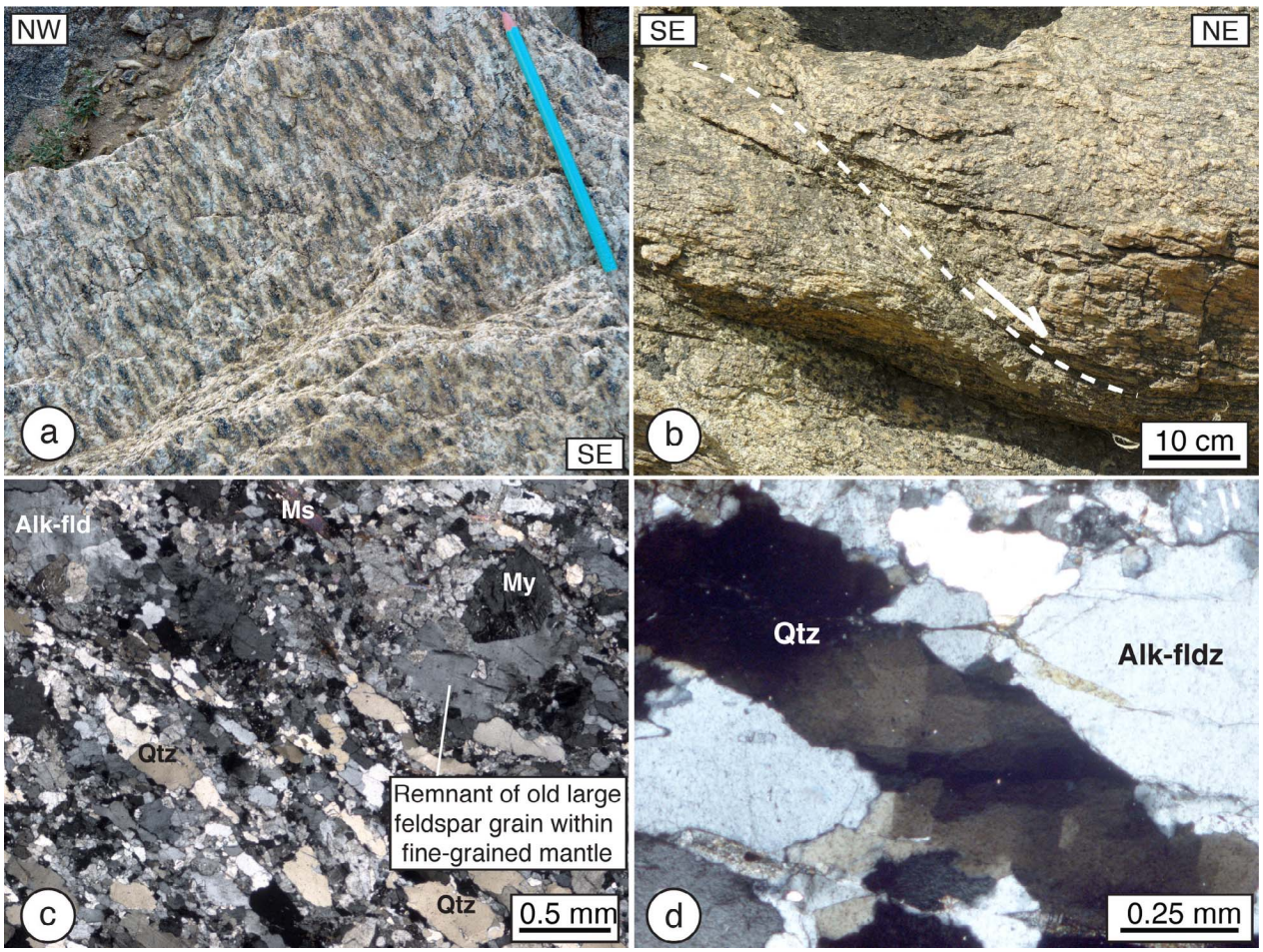

Figure 7. Photographs of solid-state fabrics from the margins of the Nartyn intrusion. (a) Well-expressed NW-SE trending mineral lineation marked by the preferred orientation of biotite aggregates. (b) Discrete shear bands observed along the northern margin of the Nartyn granite. (c and d) Cross-sections in cross-polarized light of some foliated granite samples selected within the margins of the Nartyn intrusion. Alk-fld, K-feldspar; Bt, biotite; Qtz, quartz; My, Myrmekite; Ms, Muscovite. (c) Foliated granite sample from the southeastern margin of the granite, showing limited grain size reduction. (d) Large quartz grain from Figure 7c showing chessboard extinction. See text for further explanation.

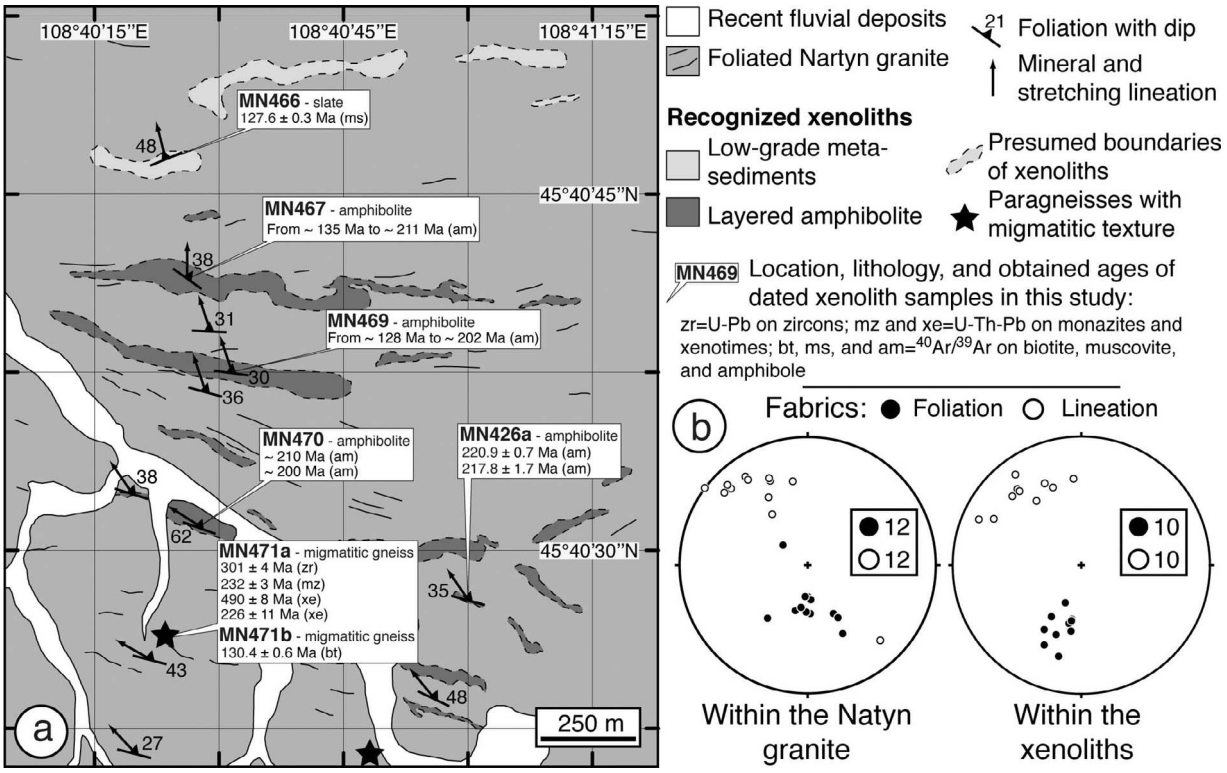

Figure 8. (a) Simplified geological map of the northern part of the Nartyn intrusion. Location in Figure 2a. Boundaries of xenoliths were drawn after field observations and satellite images from Google Earth. (b) Stereographic projections (equal area, lower hemisphere) showing ductile fabric elements (foliation and mineral and stretching lineations) measured within xenoliths and surrounding granite.

and -poor horizons, and of paragneisses and migmatites (Figure 9b) that are not observed in adjacent country rocks.

[15] Despite the scarcity of exposures of xenolith limits, field and satellite image observations indicate that they have elongate shapes of several tens to hundreds of meters in length (Figure 8a), sub-parallel to the foliation of the granite. Fabrics within xenoliths and granite show similar attitudes (Figure 8b), with foliation dipping moderately to the north and stretching and mineral lineation trending NW-SE (Figures 8b and 9a).

[16] On a north–south cross-section, xenoliths and country rock sheets show a non-random distribution, with increasing metamorphic grade from upper-crustal sedimentary rocks to migmatitic gneisses when moving downward into the

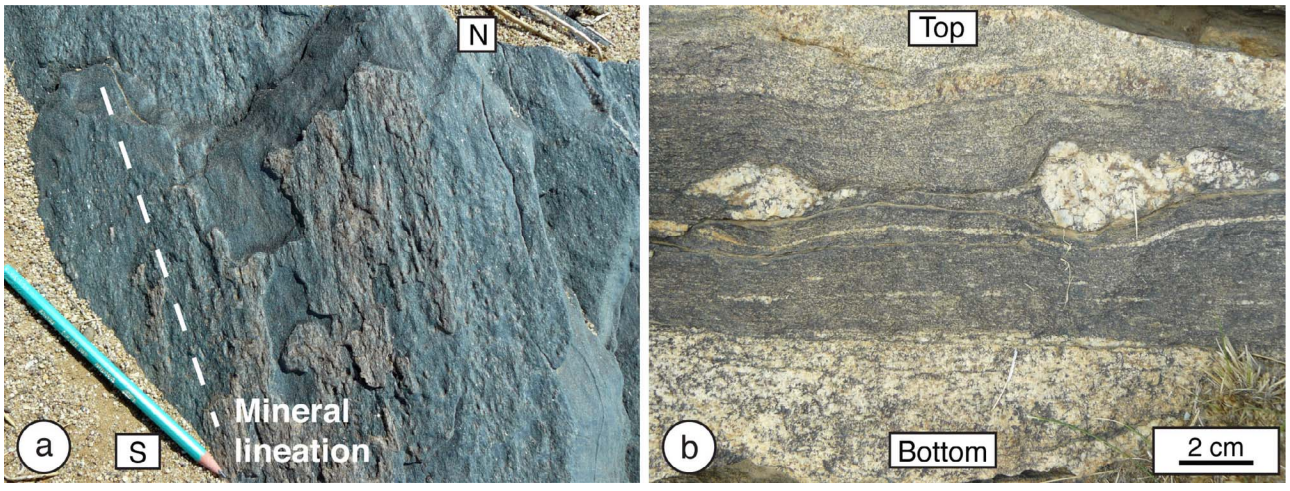

Figure 9. Photographs of xenoliths the northern part of the Nartyn granite. (a) Strong NW-SE trending mineral lineation within an amphibolite xenolith. (b) Boudinage of leucocratic vein within paragneiss xenolith.

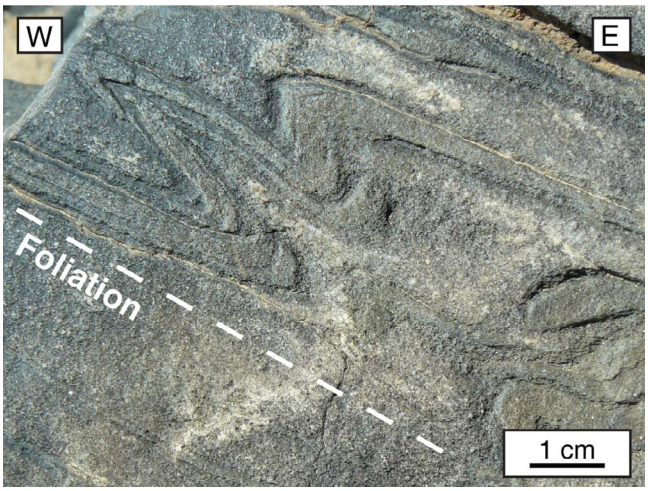

Figure 10. Amphibolite xenolith from the northern part of the Nartyn intrusion showing a folded metamorphic layering, with axial fold plane that dips gently NNW-SSE toward the granite boundary.

granite, away from the contact (Figure 8a). The xenolith layers appear to be large, thin sheets of crustal country rocks trapped by the Nartyn granite during emplacement. The overall geometry and internal fabrics further suggest some sheeted-dyke emplacement of the granite in a tectonic context involving subvertical shortening and NE-SW stretching (Figure 9a and 9b). Some places show that the moderately dipping fabric of the country rock sheets rework a more steeply dipping one (Figure 10).

3.2.4. Structure of Country Rocks

[17] Except along the Choyr Sear Zone, the Nartyn granite shows intrusive contacts with metasediments. Metasediments show a well-defined schistosity that dips outward, generally at low angle to granite contact and granite fabric (Figure 2a and 11a).

[18] Southeast of the intrusion, moving away from the contact, country rocks show a generally steeply dipping foliation (Figure 11a). The area is marked by NE-SW directed bands dominated by grayish marble alternating with bands dominated by dark blue quartzite and slate, and with bands of underlying basement. The overall geometry strongly suggests NE-SW striking folds with sub-horizontal axes (Figure 11b).

4. The Altanshiree Granite: A Comparable Intrusion

[19] At about 140 km east of the Nartyn massif, the Altanshiree area (Figure 12) comprises several granitic plutons. One of these, the Altanshiree granite, shows similar features to those of the Nartyn granite. It is a coarse-grained biotite-rich granite marked by a flat-lying magmatic fabric (Figure 13a). Along its margins, the intrusion displays solid-state foliations that dip gently outward (Figure 13b). Foliation planes bear a generally weak NW-SE to NS mineral lineation underlined by the preferential alignment of biotite and quartz-feldspar aggregates. Country rocks comprise rhyolites and amphiblolites affected by a strong flat-lying foliation (Figures 13c and 13d). Despite the strong subvertical shortening (see Figure 13d), we have not found evidence of low-angle normal shear zones as observed at the northwestern roof of the Nartyn granite.

5. Geochronology

[20] We performed geochronological analyses in order to estimate the emplacement age of the Nartyn granite, to estimate the duration of deformation events, and to constrain the cooling history of the area. U-Th-Pb chemical analyses and U-Pb isotopic analyses were performed on monazite, xenotime, and zircon. In addition, muscovite, biotite, and amphibole were analyzed through $^{40}Ar/^{39}Ar$ laser step heating experiments from various metamorphic and magmatic rocks sampled in the area. Geochronological analyses were also performed in the Altanshiree area. Sample locations are shown in Figures 2b, 8, and 12. Sample coordinates and results are reported in Tables S1, S2, and S3 in the auxiliary material.[1] Methodological approaches are also available in Text S1 of the auxiliary material.

5.1. U-Pb Dating Results

5.1.1. Nartyn Granite

[21] The Nartyn granite sample M372 contains numerous large zircon grains (>200 μm). The grains are frequently clear and display elongate- or sub-equant-shapes. Eleven analyses were performed on 9 grains. They reveal a great variety of compositions. The Th/U ratio can be very low, but it can also reach values close to 1. One analysis was omitted because the amount of common Pb was too high (Table S1). One of the two analyses performed on grain 7 appears concordant in the *Tera and Wasserburg* [1972] diagram and provides the oldest age at the Cambrian-Ordovician boundary (Figure 14a). This grain is interpreted as inherited. Grain 2 is younger, but it probably reflects inheritance as well. The remaining analyses are heterogeneous in age. Although analysis 4.1 displays a significant contribution of common Pb, it was added to the six remaining analyses that are grouped together close to the Concordia. A mean age of 133 $\pm$ 3 Ma was calculated from the intercept of Concordia with a mixing line that extends from the value of common Pb at 130 Ma (Figure 14a).

[22] In addition, this sample contains middle-size altered grains of monazite (150–300 μm) that frequently show corroded boundaries. One hundred chemical analyses were performed on 7 grains using the electron microprobe. Nine of them were discarded because they had either an oxide total lower than 97% or yielded individual ages significantly older or younger than the remaining analyses. The remaining analyses are sufficiently heterogeneous in U and Th composition to provide a well-defined regression line (Figure 14b), whose slope is similar to that of a theoretical isochron within the Th/Pb = f(U/Pb) diagram. The intercept of the regression lines with the axes of the diagram provides similar ages with a mean age of 149 $\pm$ 3 Ma calculated at the centroid of the population (Figure 14b).

5.1.2. Migmatitic Gneiss Xenolith Within the Nartyn Granite

[23] The migmatitic gneiss sample MN471a from a xenolith within the Nartyn intrusion contains small (100–200 μm)

[1] Auxiliary materials are available in the HTML. doi:10.1029/2011TC002926.

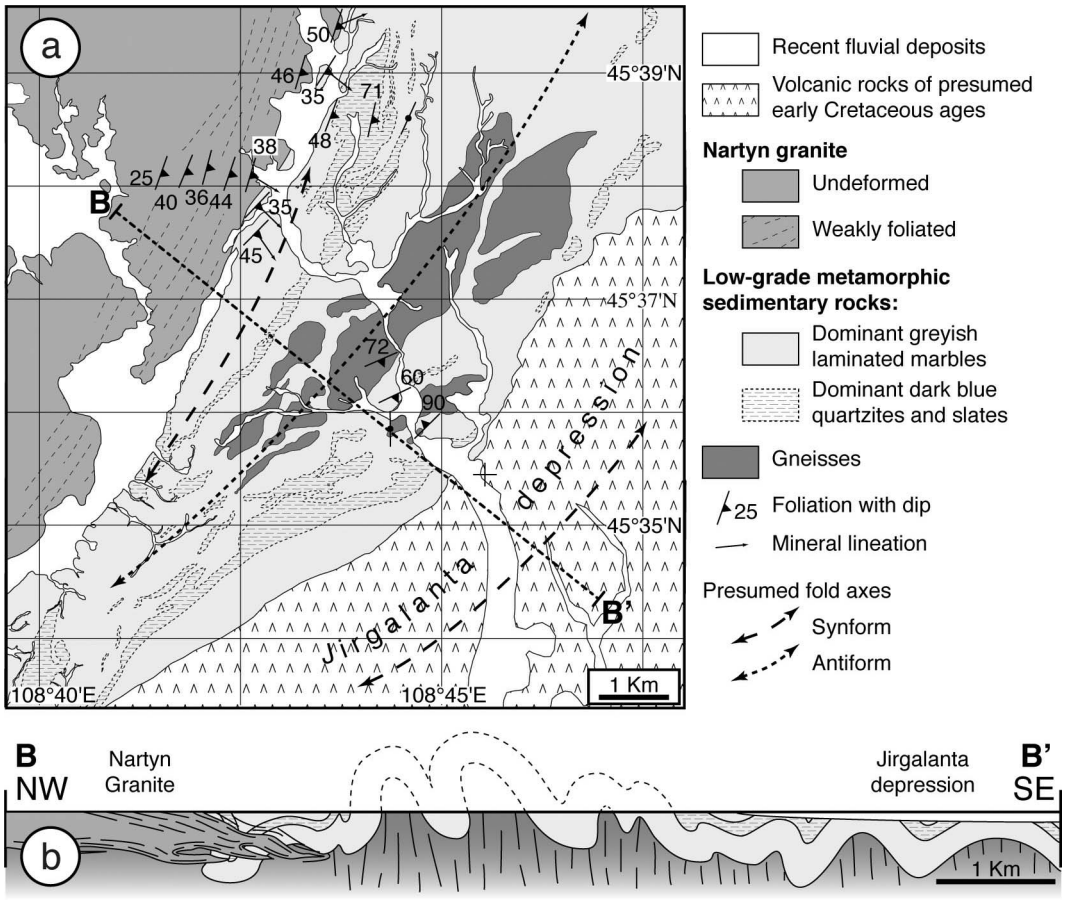

Figure 11. (a) Simplified geological map of the southeastern part of the Nartyn massif. Location in Figure 2a. (b) Interpretative cross-section. Location in Figure 11a.

dark and milky zircon grains. Thirteen analyses were carried out on 9 grains. Three of them yielded the oldest ages at ca 900–1000 Ma in the *Tera and Wasserburg* [1972] diagram (Figure 14c). Nine other analyses provided Phanerozoic ages. However, two of them (8.1 and 9.1) were discarded because they show significant contributions in common Pb. Although analysis 6.1 overlaps with Concordia, it is older than the remaining analyses and it may reflect inheritance. Two additional analyses (2.1 and 1.1) display disturbances that might be attributed to radiogenic Pb-loss. The remaining analyses allow a mean age of 301 ± 4 Ma to be calculated.

[24] One hundred chemical analyses were performed on 4 grains of monazite that are characterized by euhedral-shapes. Seventeen analyses were discarded because they have total oxide amounts lower or higher than the range 97–103%, respectively. Nine additional analyses that yielded significantly older ages were also rejected. The remaining data set permits the calculation of a regression line with a slope similar to that of the theoretical iscochron at 232 Ma (Figure 14d). The intercepts of the regression line with the axes of the diagram being identical in their individual errors, a mean age of 232 ± 3 Ma was calculated at the centroid of the population.

[25] The sample also contains euhedral grains of xenotime (100–250 μm) that are rich in inclusions. Most of these grains display core-rim internal textures. Two hundred and forty chemical analyses were performed on 12 grains. Among them, 37 were rejected because their oxide totals were lower than 97%. The remaining analyses were separated into two distinct populations at ∼500 Ma and ∼230 Ma (Figures 14e and 14f). The oldest group was obtained from 72 analyses of xenotime grain cores. In the Pb = f(U*) diagram [see *Suzuki and Adachi*, 1991], these data spread along a regression line that provides a mean isochron age of 490 ± 8 Ma. Ninety analyses made on grain rims provide a well-constrained isochron that yields a mean age of 226 ± 11 Ma. This latter regression line was not forced through the origin. Thus, its intercept with the *y* axis is attributed to the occurrence of common Pb. Indeed, previous studies have shown that xenotime may contain significant amounts of common Pb [*Cocherie and Legendre*, 2007].

5.1.3. Altanshiree Granite

[26] The granite sample M357a from the Altanshiree intrusion contains numerous elongate or thick, medium-sized grains of zircon (∼200 μm). Most grains are clear, but some appear smoky. Thirteen analyses carried out on 10 grains reveal a large scattering of U and Th concentrations, as well as in Th/U ratio (see Table S1). Analysis 2.1 was removed because of its high U concentration. Analysis 8.1 was also rejected because it is shifted, due to significant Pb-loss. The remaining analyses display scattered ages in the *Tera and Wasserburg* [1972] diagram (Figure 14g). This feature might suggest that zircon crystallized at different times: 253 ± 6 Ma, 146 ± 3 Ma, and 127 ± 7 Ma. The two oldest

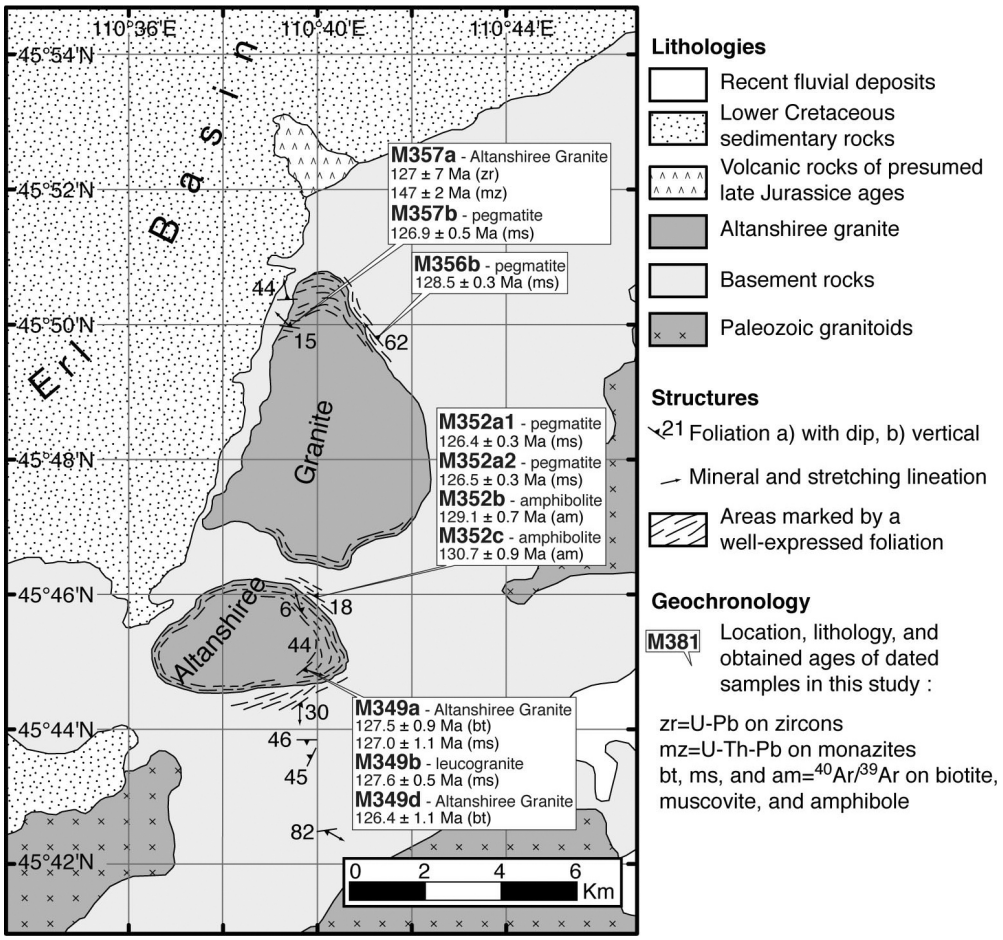

Figure 12. Simplified geological map of the Altanshiree area. Location on Figure 1. Locations of samples used for geochronological analyses are indicated.

calculated mean ages might be attributed to inheritance. Thus, the youngest mean age might be interpreted as that of granite emplacement. Alternatively, the mean age of 146 ± 3 Ma may instead be that of the granite emplacement, and the youngest mean age might reflect significant radiogenic Pb-loss undergone by some zircons.

[27] This sample contains large euhedral grains of monazite (300–500 μm) that are marked by the occurrence of contrasting domains. One hundred and thirty chemical analyses were performed on 7 grains. Three were rejected because they display total oxides lower than 97%. Six additional analyses were removed because they were statistical outliers. The remaining data set is plotted on the Th/Pb = f(U/Pb) diagram (Figure 14h) in which a regression line may be determined. The slope of the line is similar to that of the theoretical isochron at ~147 Ma. The intercepts of the regression line with the axes of the diagram are comparable in age in the limit of their individual errors. Thus, a mean age of 147 ± 2 Ma was calculated at the centroid of the population.

5.2. $^{40}Ar/^{39}Ar$ Results

5.2.1. The Nartyn Area

5.2.1.1. Nartyn Granite

[28] Within the granite, while most of mica age spectra of undeformed to poorly deformed coarse-grained biotite (MN327 and MN378) and foliated muscovite-rich granite samples (MN392) allow plateau age calculations in the range 130.8 ± 0.5 Ma to 129.5 ± 0.3 Ma, muscovite MN464 from a leucocratic granite yielded a slightly saddle-shaped age spectrum and a younger plateau age at 127.7 ± 0.2 Ma (Figures 15a and 15d). Dykes of microgranite (MN275) and pegmatites (M374 and MN322b) yielded mica plateau ages in a similar narrow time range from 130.2 ± 0.4 Ma down to 128.9 ± 0.9 Ma (Figures 15b and 15c).

5.2.1.2. Xenoliths

[29] Micas from xenoliths of quartzite (MN463), slate (MN466b), and migmatitic gneiss (MN471b), included in the Nartyn granite, yield plateau ages between 130.4 ± 0.6 Ma and 127.4 ± 0.4 Ma (Figures 16a and 16b). Age spectra of amphiboles are more complex and their disturbances are probably related to granite intrusion, as suggested by mica ages and by some of the low temperature apparent ages in the amphibole spectra. Amphibole age spectra from amphibolite samples MN467 and MN469 (Figure 16c) suggest partial recrystallization at ~130 Ma, after an initial (re)crystallization phase that occurred before ~210 Ma. Remnants of a late Triassic event are corroborated by the two amphibole plateau ages at ~220 Ma from amphibolite sample MN426a (Figure 16d). Despite excess argon incorporation indicated by the shape of their age spectra, the two amphiboles of amphibolite xenolith MN470 that yielded late Triassic ages at

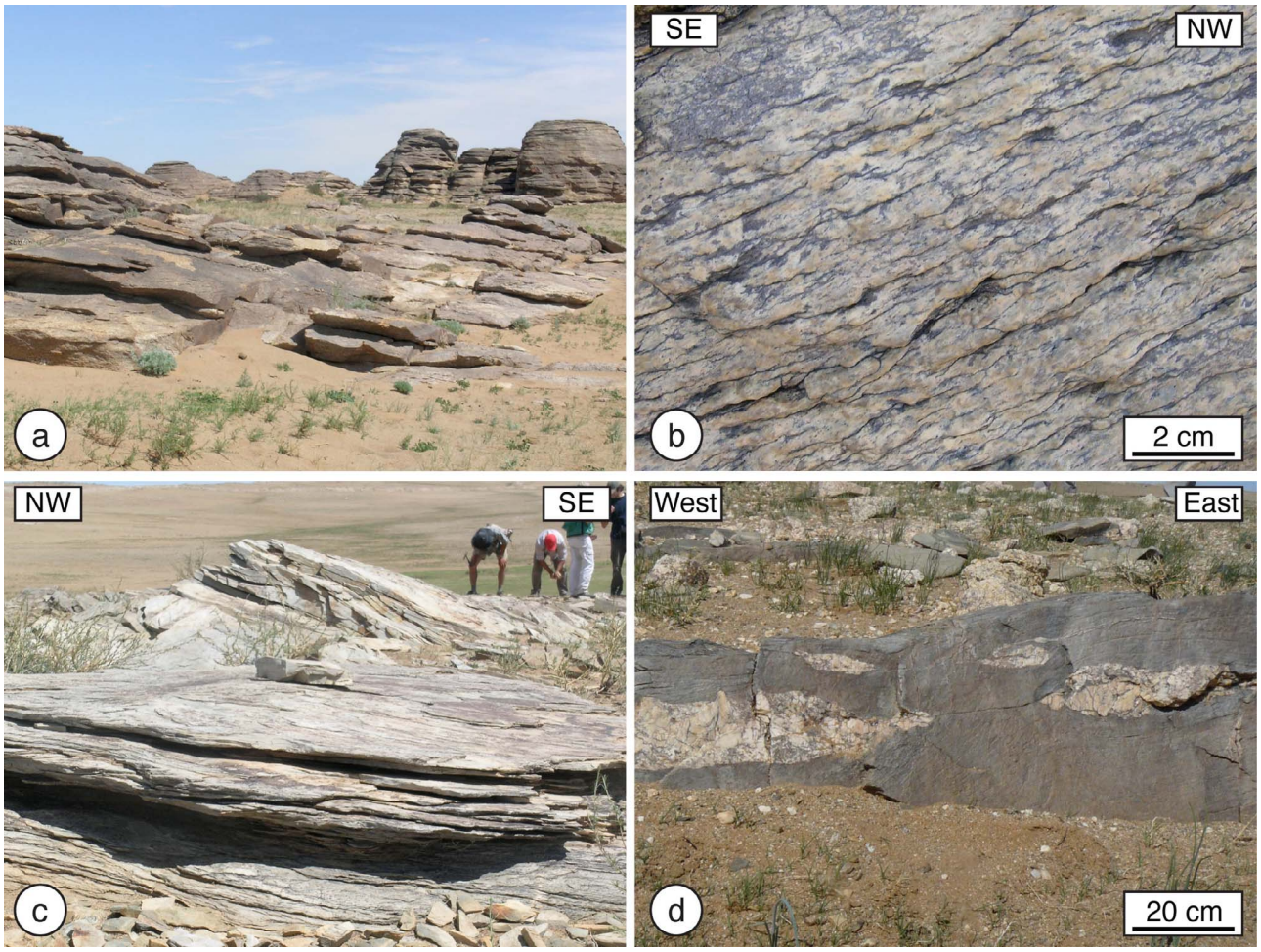

Figure 13. Structural features from the Altanshiree area. (a) Pervasive flat-lying fabric within the Altanshiree intrusion. (b) Fabrics at the southern margin of the intrusion. (c) Flat mylonitic foliation within rhyolitic country rocks. (d) Boudinaged leucocratic dykes within amphibolite country rocks.

fusion steps also suggest a (re)crystallization at ~210–220 Ma (Figure 16e). An intermediate age of ~160 Ma from amphibole MN404 (Figure 16f) sampled within a mafic xenolith suggests excess argon, which seems to be confirmed by correlation diagram ($^{36}Ar/^{40}Ar$ versus $^{39}Ar/^{40}Ar$) [*Turner*, 1971; *Roddick et al.*, 1980; *Hanes et al.*, 1985]. Nevertheless, age spectrum flatness over ~80% of ^{39}Ar degassing, and small age difference between calculated plateau and isochron ages, respectively 160.2 ± 0.5 Ma and 157.5 ± 0.8 Ma ($(^{40}Ar/^{36}Ar)_i$ = 347.3 ± 7.3 and MSWD = 1.7), suggest that the isochron age of ~157.5 Ma might be a good estimate for cooling or (re)crystallization of this amphibole.

5.2.1.3. Nartyn Granite Vicinity

[30] Among the nine micas that were separated from samples collected within the low-grade metasedimentary cover and leucogranite and pegmatite dykes in the vicinity of the Nartyn intrusion (Figure 2b), seven (samples MN321c, MN375, M371a2, M371a1, and M371a3) yielded plateau ages distributed between 132.3 ± 0.3 Ma and 128.4 ± 0.4 Ma (Figures 17a, 17b, and 17c).

[31] A muscovite from a quartz-feldspar vein (M369) collected within the Jirgalanta depression yielded a characteristic saddle-shaped age spectrum (Figure 17d), which expresses partial recrystallization with distinctive degassing patterns of inherited and recrystallized domains [e.g., *Cheilletz et al.*, 1999; *Tremblay et al.*, 2000; *Castonguay et al.*, 2001; *Alexandrov et al.*, 2002]. According to *Alexandrov et al.* [2002], such a spectrum suggests that initial crystallization would have occurred before ~151–152 Ma (apparent age at fusion step), possibly at ~157 Ma; the saddle minimum at ~141 Ma may represent a maximum age estimate for a recrystallization or a secondary crystallization of muscovite. However, the first 6.5% of ^{39}Ar degassing with a mean age at 136.4 ± 1.7 Ma are probably the best estimate for the age of recrystallization.

[32] Two muscovites from slate M352a and pegmatite M353a yielded significantly older plateau and pseudo-plateau ages at 208.5 ± 0.4 Ma and 217.0 ± 0.4 Ma, respectively (Figure 17e). Such a late Triassic age, comparable to ages observed for amphibole age spectra from xenoliths within the Nartyn intrusion, was also recognized for the amphibole MN366 plateau age at ~216 Ma (Figure 17f).

[33] Finally, three other strongly disturbed age spectra obtained from an amphibole in a skarn (MN356a) and from micas collected within the crystalline basement (MN315 and

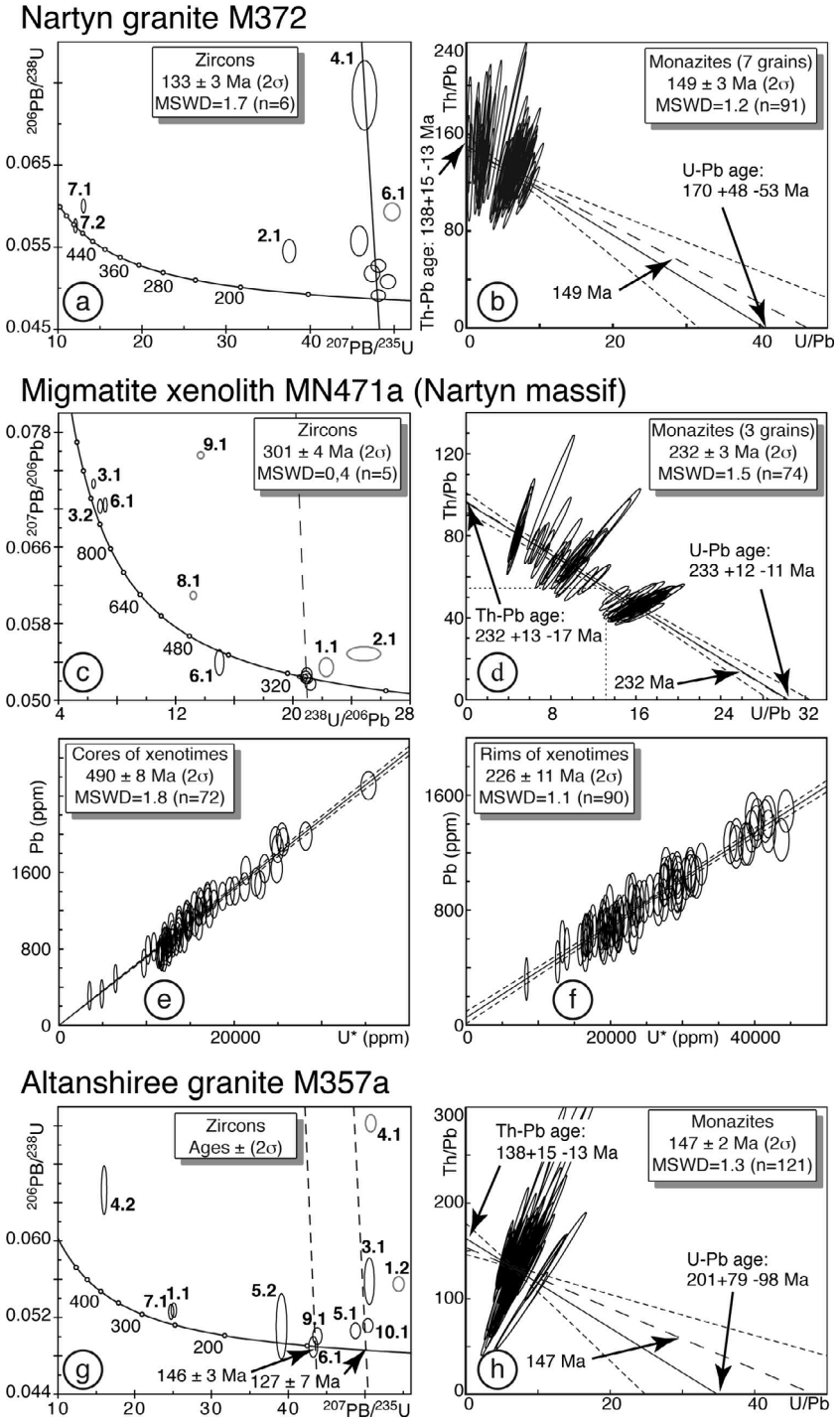

Figure 14. U-Pb data for the Nartyn and Altanshiree areas. Sample locations in Figures 2b, 8a, and 12. (a) *Tera and Wasserburg* [1972] Concordia diagram for zircons of the Nartyn granite. (b) Th/Pb versus U/Pb diagram for monazites from the Nartyn granite. *Tera and Wasserburg* [1972] Concordia diagram for (c) zircons, (d) Th/Pb versus U/Pb diagram for monazites, and (e, f) Pb versus U* diagrams for xenotimes of migmatite xenolith from the northern part of the Nartyn granite. *Tera and Wasserburg* [1972] Concordia diagram for (g) zircons and (h) Th/Pb versus U/Pb diagram for monazites from the Altanshiree granite. See the methodological approach in the auxiliary material and text for further explanations.

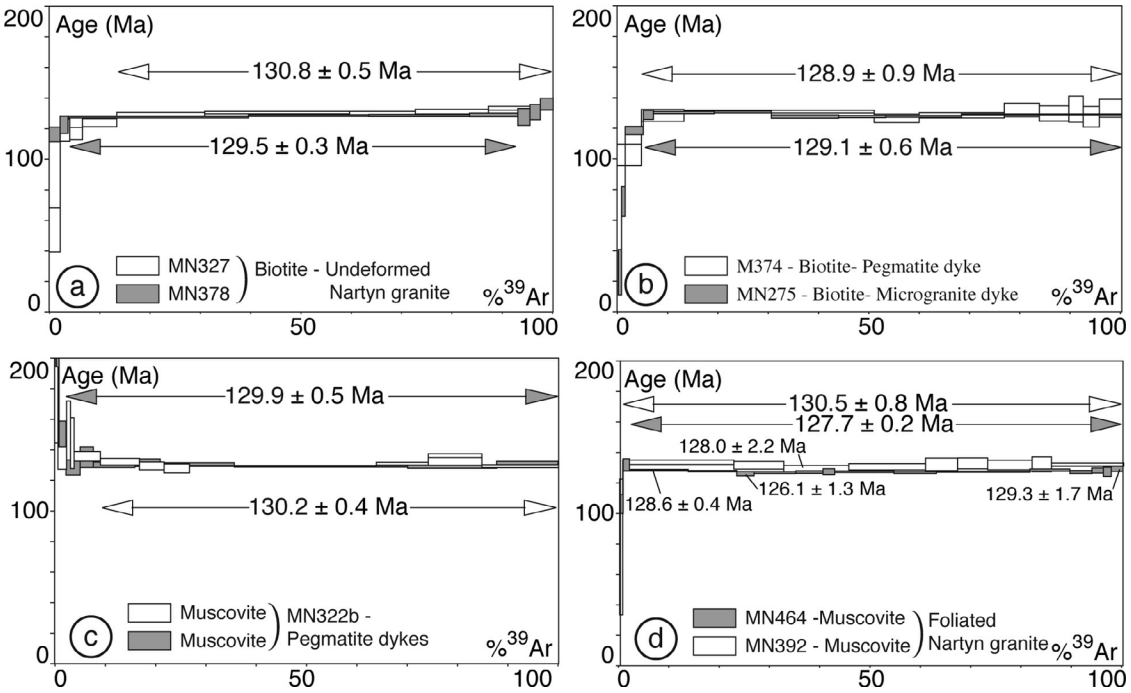

Figure 15. (a–d) $^{40}Ar/^{39}Ar$ age spectra for micas from the Nartyn granite. Sample locations in Figure 2b. See the methodological approach in the auxiliary material and text for further explanations. The age error bars for each temperature steps are at 1σ level. The errors in the J-values are not included. Plateau ages were calculated at the 2σ level taking into account errors on the J-values, but they are shown with 1σ uncertainties.

MN319a) suggest that some domains of the country rocks could be older than ~360 Ma (Figures 17f and 17g).

5.2.1.4. Choyr Shear Zone

[34] All micas collected within the Choyr Shear Zone (Figure 2b) yielded flat age spectra allowing plateau age calculations in a narrow but significant time range of ~3–4 Myr from 129.0 ± 1.4 Ma to 125.3 ± 0.5 Ma (Figure 18), without age differences between muscovite and biotite. Among the four analyzed amphibole grains, two from a mafic rock M381 and an orthogneiss M401a yielded plateau ages at 138.2 ± 0.4 Ma and 128.7 ± 0.3 Ma (Figures 18e and 18f). Age spectrum provided by an amphibole from orthogneiss MN302 provided an intermediate plateau age at 135.2 ± 1.3 Ma (Figure 18g). However, this result is ambiguous because apparent ages decrease slightly from the low to the high temperature steps, which could suggest excess argon. This is corroborated by calculations using correlation diagram with a $(^{40}Ar/^{36}Ar)_i$ ratio at 482.9 ± 95.2 (MSWD = 1.3), which is significantly higher than atmospheric ratio. It provides an isochron age of 132.0 ± 1.3 Ma, which is significantly younger than the plateau age. We consider this isochron age as a maximum estimate of the true age of the amphibole. The fourth amphibole from orthogneiss MN401b, displays a hump-shaped age spectrum (Figure 18h), whose rather flat intermediate degassing temperature domain suggests an initial (re)crystallization before ~200 Ma.

5.2.2. $^{40}Ar/^{39}Ar$ Results From the Altanshiree Area

[35] The two amphiboles from amphibolites M352b and M352c sampled within host rocks of the Altanshiree granite yielded nearly concordant ages at 130.7 ± 0.9 Ma and 129.1 ± 0.7 Ma (Figure 19a). Micas (mainly muscovites) from samples collected within the Altanshiree intrusion (foliated granite M349a and M349d, leucogranite M349b, and pegmatites M356b and M357b) and within country rocks (pegmatites M352a1 and M352a2) provided younger plateau ages in the range 128.5 ± 0.3 Ma to 126.4 ± 0.3 Ma (Figures 19b, 19c, and 19d).

6. Interpretation

6.1. Mechanism of Granite Emplacement

[36] There are no geophysical data available to constrain the shape of the Nartyn and Altanshiree intrusions. However, the granite-xenolith relationships observed in the northern part of the Nartyn massif (Figure 8) point to local sheeted geometries, and a most remarkable character of both Nartyn and Altanshiree granites is the occurrence of sub-horizontal magmatic fabrics (Figures 6a and 13a), often weak but pervasive throughout the intrusions. These features are consistent with a geometrical interpretation of a thin, elongate, laccolith-type body (Figure 20).

[37] The pervasive flat fabrics observed in the Nartyn and Altanshiree intrusions, the normal Choyr Shear Zone, the lower Cretaceous Choyr Basin in the hanging wall of the shear zone, and the strong sub-horizontal foliations that characterize xenoliths within the Nartyn granite and country rocks close to both intrusions (Figures 9b, 13b, and 13c) show that prominent structures developed in the region resulted from extensional deformation and crustal thinning.

[38] Within the northern part of the Nartyn granite, the sheets and panels of high-grade metamorphic rocks present fabrics comparable to those within the intrusion (Figure 8b).

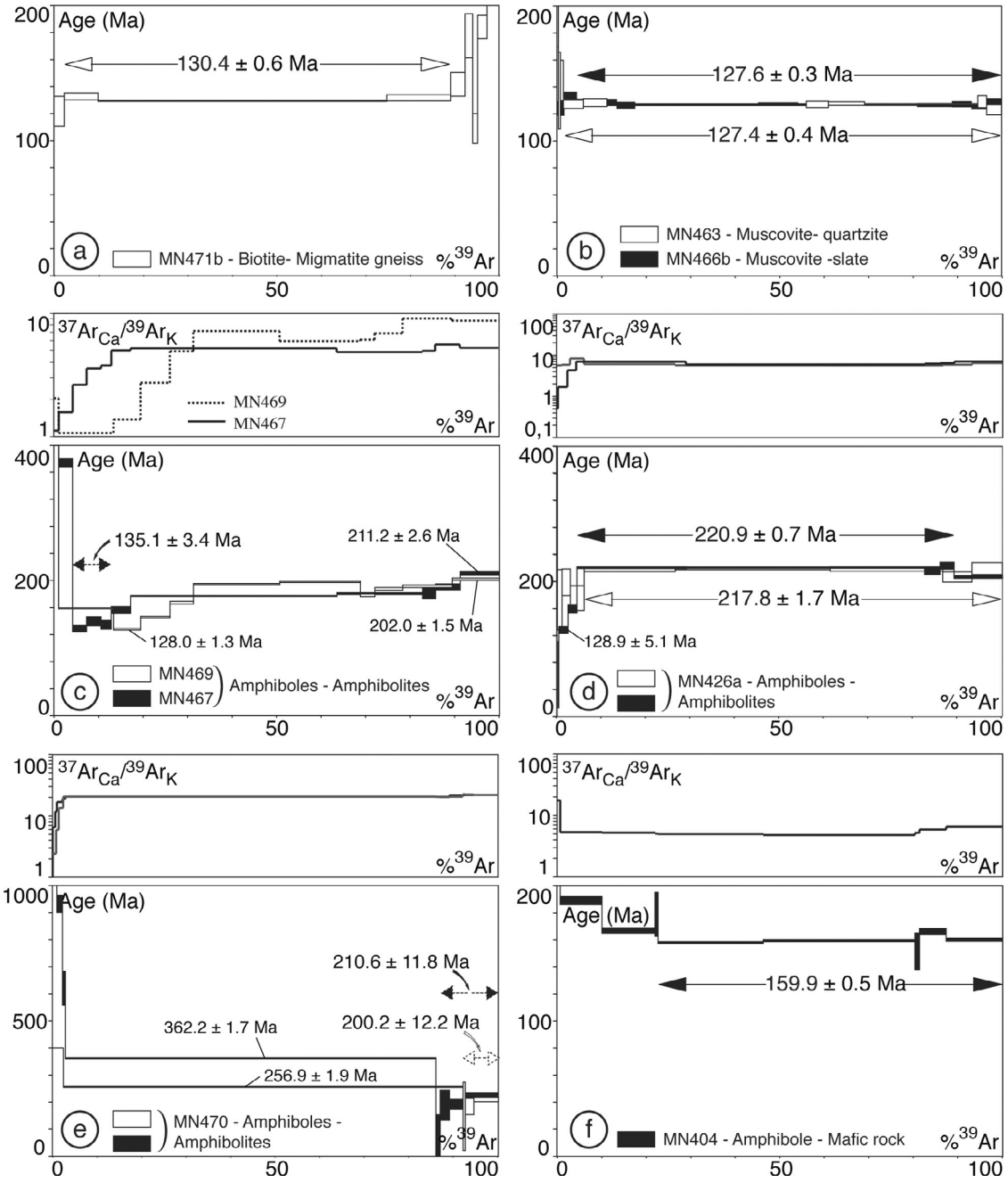

Figure 16. (a–f) $^{40}Ar/^{39}Ar$ age spectra for micas and amphiboles from xenoliths within the northern part of the Nartyn granite. Sample locations on Figures 2b and 8a. See the methodological approach in the auxiliary material and text for further explanations. The explanations of error calculations are given in caption of Figure 15.

In the field, fabrics within the xenoliths appear often stronger than that of the surrounding granite, with locally intense folding of a pre-existing fabric (Figure 10). This suggests that the flat-lying xenolith fabrics developed prior to intrusion emplacement and thus xenoliths appears as witnesses of the underlying ductile metamorphic crust. Steeply dipping foliations comparable to those found as remnants in the xenoliths are observed southeast of the Nartyn granite, away from the contact (Figure 11). Furthermore, $^{40}Ar/^{39}Ar$ ages in this area (~346–359 Ma, Figure 2b) support the interpretation that steep foliations reflect an older deformation event that occurred prior to extension.

[39] Features above underline that country rocks of xenoliths in the northern part of the Nartyn granite have been reworked by ductile extensional deformations; whereas those observed to the South were not. From this, we infer that the Nartyn granite was emplaced near the brittle-ductile transition (Figure 20). The vicinity of the Nartyn granite from the brittle-ductile transition during extension is supported by $^{40}Ar/^{39}Ar$ age spectra of micas and most amphiboles from the

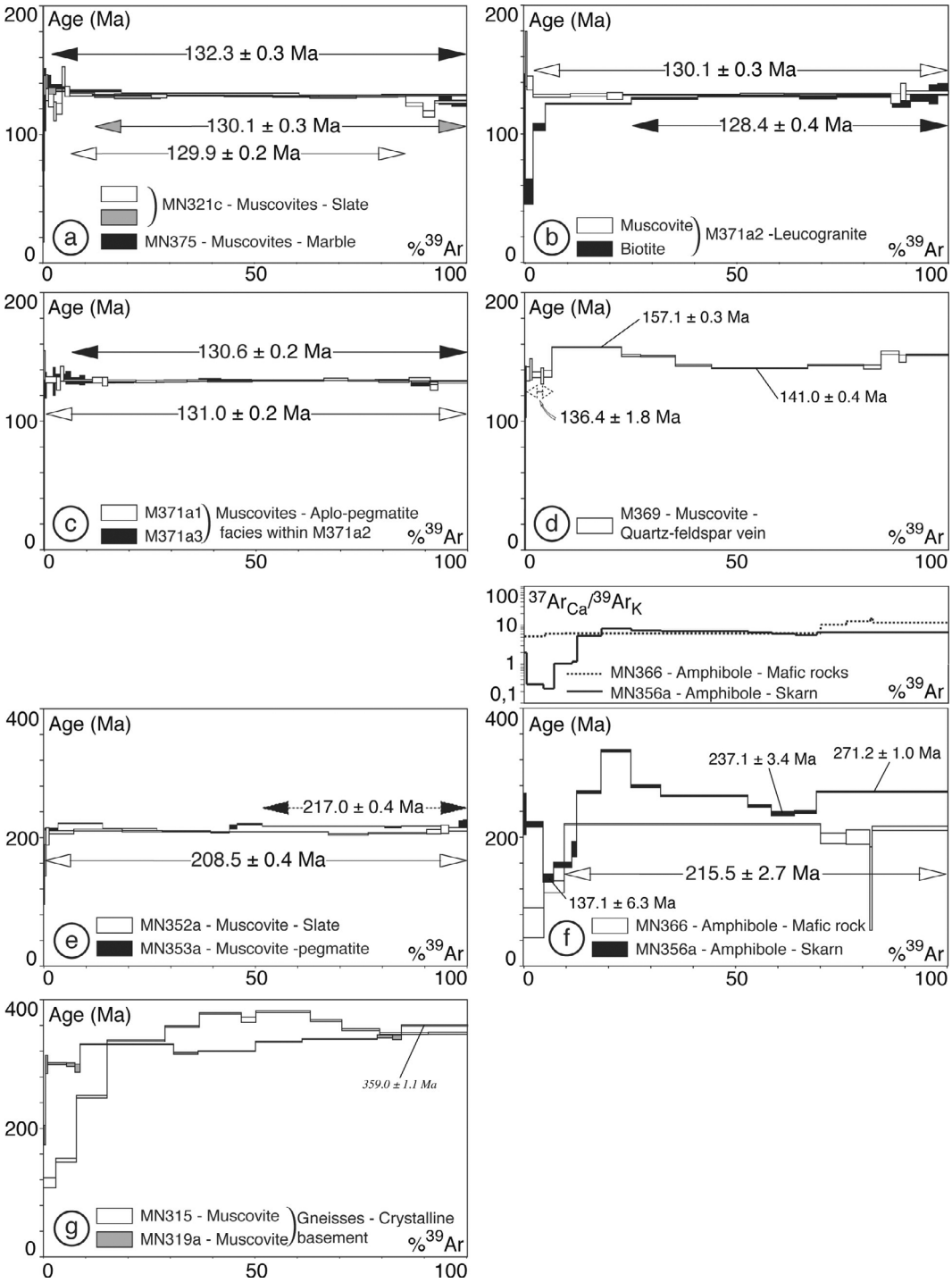

Figure 17. (a–g) $^{40}Ar/^{39}Ar$ age spectra for micas and amphiboles from country rocks the Nartyn granite. Sample locations in Figure 2b. See the methodological approach in the auxiliary material and text for further explanations.

Choyr Shear Zone and xenolith sheets to the north of the Nartyn intrusion that show partial resetting and early cretaceous plateau ages; whereas the southeastern country rocks away from the intrusion provided old ages (Figure 2b). The general metamorphic and structural pattern of the Nartyn area would thus imply (1) strong squeezing of isograds between rocks from the Choyr Shear Zone and the granite country rocks to the south as a result of sub-vertical shortening, and (2) southward tilting of the Choyr Shear Zone footwall during late stages of normal shearing (Figure 20).

[40] Around the Altanshiree intrusion, where no low-angle normal shear zone was observed, country rocks show strong flat-lying fabrics (Figures 13c and 13d), consistent with those observed in the granite (Figures 13a and 13b), which indicates that extensional deformation was accommodated by pervasive crustal thinning.

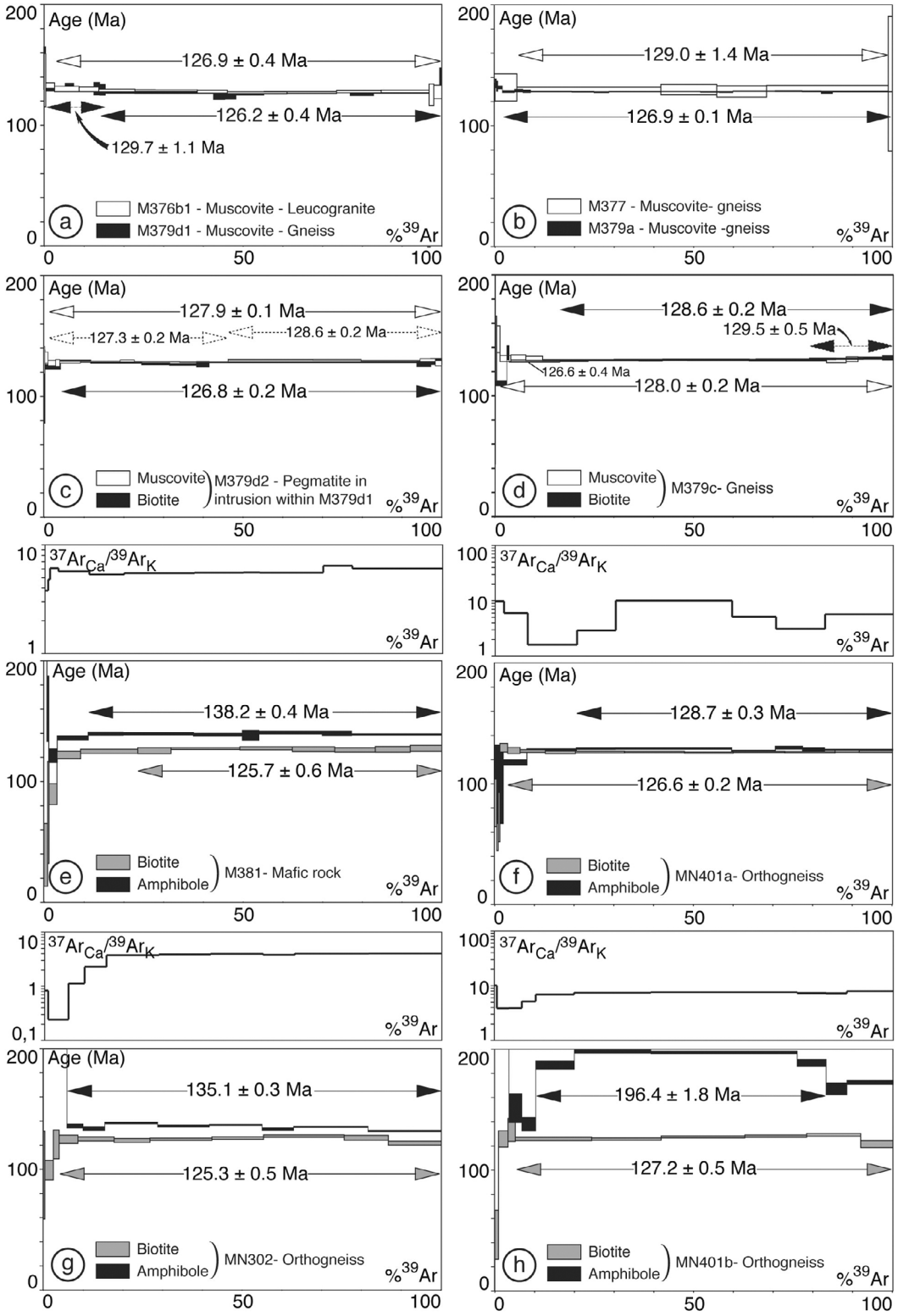

Figure 18. (a–h) $^{40}Ar/^{39}Ar$ age spectra for micas and amphiboles from the Choyr Shear Zone. Sample locations in Figure 2b. See the methodological approach in the auxiliary material and text for further explanations. The explanations of error calculations are given in caption of Figure 15.

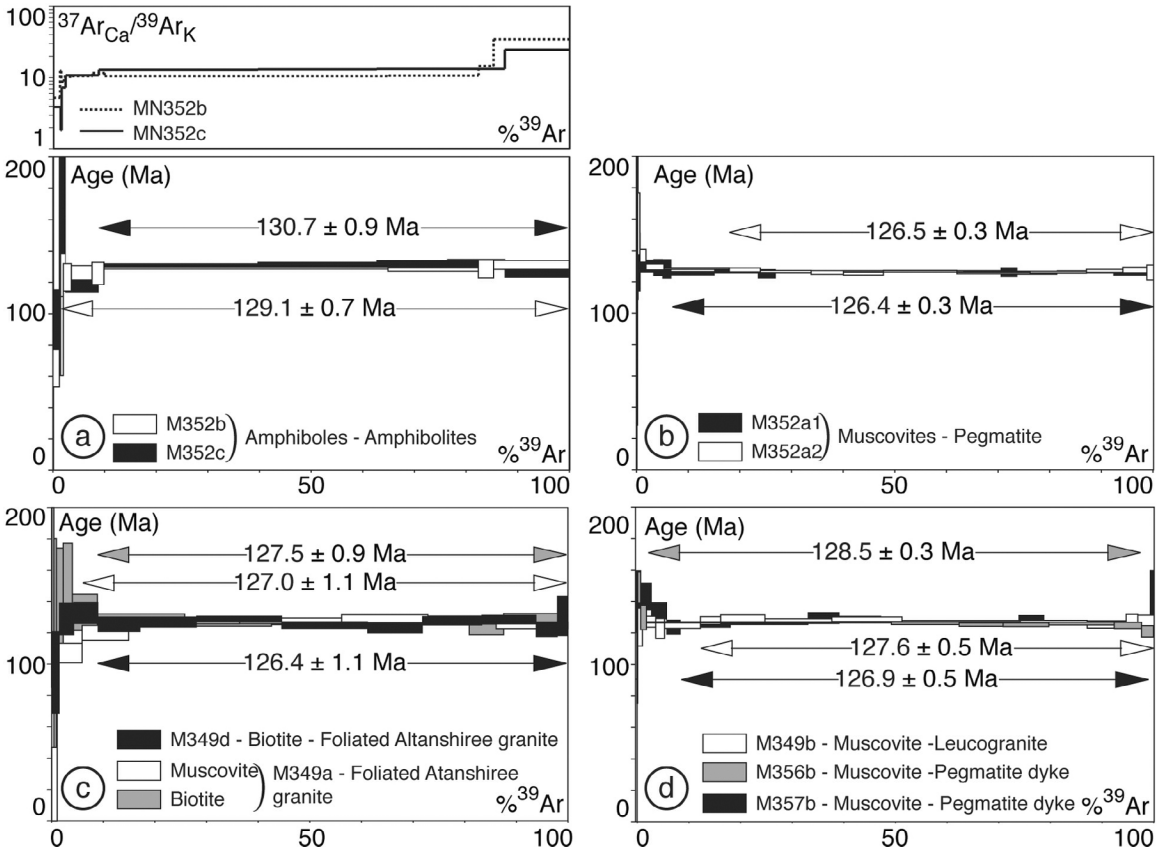

Figure 19. (a–d) $^{40}Ar/^{39}Ar$ age spectra for micas and amphiboles from the Altanshiree granite and country rocks. Sample locations in Figure 12. See the methodological approach in the auxiliary material and text for further explanations. The explanations of error calculations are given in caption of Figure 15.

[41] In classical metamorphic core complexes, extension is mainly expressed by a detachment leading to the exhumation of hot middle to lower crust in its footwall [e.g., *Davis*, 1983; *Miller et al.*, 1983], as documented in analogue and numerical models [e.g., *Brun*, 1999; *Tirel et al.*, 2004]. In the case of Nartyn and Altanshiree areas, extension instead appears to show mixed modes between strongly localized deformation, as in mature core complexes, and strongly distributed deformation with pervasive crustal thinning, which as been only rarely documented in nature [e.g., *Cagnard et al.*, 2004]. This may indicate that the pre-extension brittle crust was particularly thin and/or that the amount of bulk horizontal stretch remained limited. The latter hypothesis is not clearly supported by our field observations. We thus favor the interpretation of a thin brittle crust, which implies limited necking effect during extension-induced boudinage of the brittle crust.

6.2. Emplacement Ages of the Nartyn and Altanshiree Intrusions

[42] The youngest zircons from the M372 Nartyn granite sample yielded a U-Pb zircon age of 133 ± 3 Ma (Figure 14a) that is interpreted as the emplacement age of the intrusion. More accurate $^{40}Ar/^{39}Ar$ ages from micas of magmatic rocks that crop out within the Nartyn intrusion (Figures 2b and 15), and within the slightly deformed country rocks close to the southeastern contact of the granite (Figures 2b and 17) suggest that cooling occurred at least until ~132–129 Ma

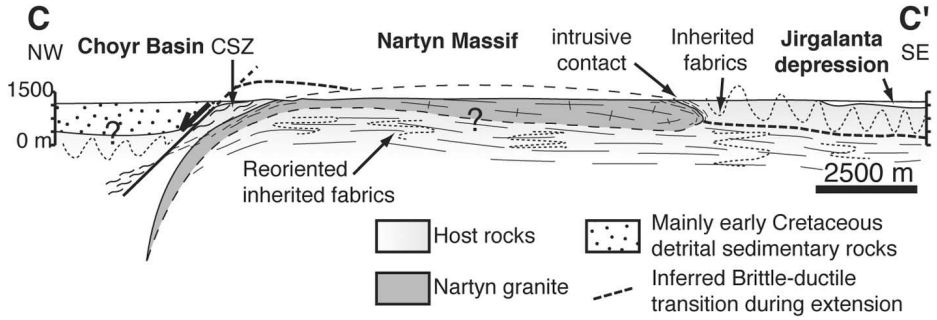

Figure 20. Interpretative NW-SE cross-section of the Nartyn area.

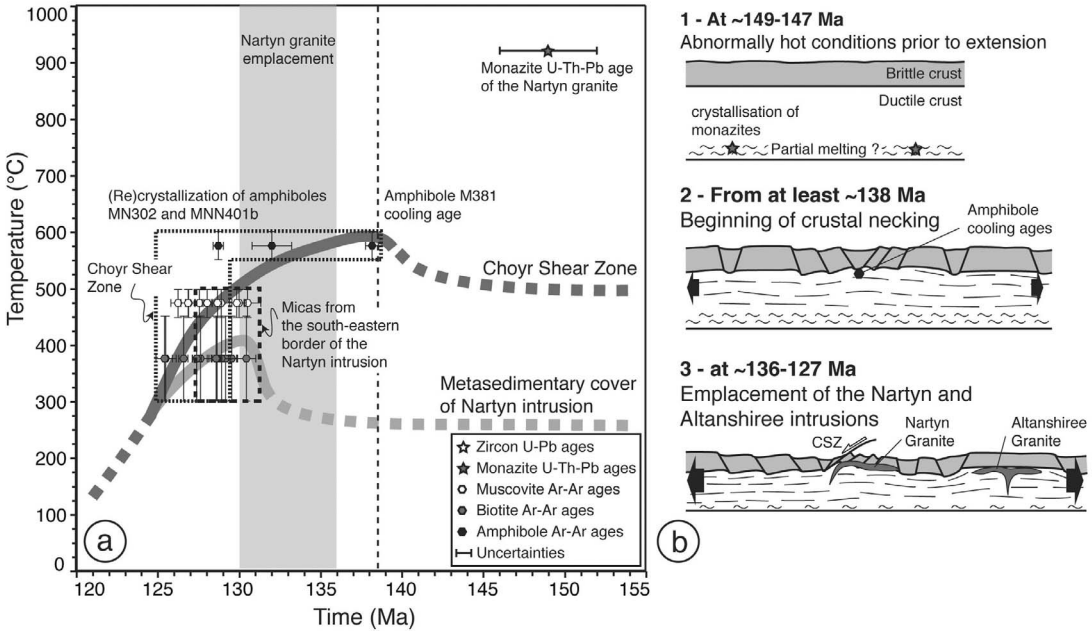

Figure 21. (a) Possible thermal evolution of the Nartyn massif. Assumed $^{40}Ar/^{39}Ar$ closure temperatures are 575 ± 25°C for amphiboles, 375 ± 75°C for biotites, and 475 ± 25°C for muscovites (see Text S1 for further explanations). U-Pb zircon and U-Th-Pb monazite age errors are at 2σ levels. All $^{40}Ar/^{39}Ar$ age errors are displayed at the 1σ level. The age scattering of muscovites probably expresses combination of cooling and fluid-induced recrystallization during development of the Choyr Shear Zone (see text for further explanations). Inferred dark and graypaths are for cooling of rocks within the Choyr Shear Zone and the country rocks of the Nartyn intrusion, respectively. (b) Proposed evolution of extensional history in the study area.

(Figure 21). However, a muscovite-rich granite (MN464) and a quartzite xenolith (MN463), both located at the northern margin of the Nartyn granite, yielded significantly younger ages at ~127 Ma (Figures 2b, 15b, and 16b). A straightforward interpretation of data is that the U/Pb ages reflect the emplacement and that the $^{40}Ar/^{39}Ar$ ages indicate cooling below the closure temperature of muscovite. However, the relatively large range of mica ages from about 132 Ma to 127 Ma suggests that the cooling history of the area might have been complex, perhaps involving successive granitic pulses or fluid circulations. The muscovite age spectrum from a quartz-feldspar vein (M369) collected within the Jirgalanta depression to the southeast of the Nartyn massif (Figure 2b) also suggests that the crust was subjected to thermal activity since at least ~136.5 Ma.

[43] Within the Altanshiree granite, the youngest zircons from sample M357a yielded a U-Pb age of 127 ± 7 Ma (Figure 14g) that we consider as the age of intrusion emplacement. On the other hand, mica $^{40}Ar/^{39}Ar$ ages range from ~128–126 Ma (Figures 12 and 19b, 19c, and 19d). From these, we infer that the Altanshiree granite must have emplaced in the time range 134–128 Ma. Consistently, the 130.7 ± 0.9 Ma and 129.1 ± 0.7 Ma (re)crystallization ages of two amphiboles (M352b and M352c) (Figure 19a) collected within mafic country rocks close to the intrusion boundary (Figure 12) could reflect the early stage of cooling of host-rocks at the vicinity of the Altanshiree granite. Finally, the ~127–126 Ma muscovite crystallization or cooling ages yielded by leucogranite dykes (M352a1 and M352a2) (Figure 19b) from the same area are concordant with the ages yielded by samples collected within the Altanshiree granite and could characterize late stages of the magmatic activity and cooling in the area.

6.3. Age of the Choyr Shear Zone

[44] Three of the four amphiboles from the Choyr Shear Zone yielded early Cretaceous plateau and isochron ages that define a ~10 Myr time range, from ~138–129 Ma (Figures 2b and 18e, 18f, and 18g). It is noteworthy that the amphibole with the oldest age (M381) was sampled within rocks where amphiboles appear undeformed and do not show evidence of recrystallization, whereas those that yielded younger ages were selected from rocks that show numerous accessory minerals such as epidote and titanite, as well as late fracturing calcite infilling indicating post-crystallization fluid infiltration. Furthermore, these youngest amphiboles appear as aggregates of grains marked by irregular boundaries and the occurrence of many drops of quartz or albite, suggesting recrystallization processes. This means that if the older amphibole age is interpreted as a cooling age, it records early stages of development of the Choyr Shear Zone at ~138 Ma prior to the emplacement of the Nartyn intrusion, whereas the younger ages reflect subsequent disturbances related to shear zone evolution (Figure 21).

[45] The time range defined by muscovite age spectra is more restricted at ~129–126 Ma and significantly younger than that provided by amphiboles (Figures 2b, 18a, 18b, 18c, 18d, and 21). The 6 analyzed muscovites yield plateau ages,

but three of them show a discreet saddle shape (M376b1, M379c, and M379d1) (Figures 18a and 18d) while another is slightly staircase-shaped (M379d2) (Figure 18c), suggesting protracted recrystallization history linked to deformation and/or fluid circulation [*Castonguay et al.*, 2007]. According to interpretations proposed by *Cheilletz et al.* [1999] and *Alexandrov et al.* [2002], initial crystallization would have occurred at ~128.5–129 Ma, whereas the saddle minima with lowest apparent ages at ~125.5 Ma would represent the end of recrystallization and isotopic closure. The staircase-shaped age spectrum (M379d2), with apparent age from ~126 Ma up to ~128.5 Ma probably reflects a similar phenomenon.

[46] Unlike the ~138–135 Ma to 129–125 Ma time range defined by amphibole-biotite couples (Figures 2b, 18e, and 18g), which mainly characterizes cooling, the ~129–125 Ma range given by muscovites most probably reflects the final development of the Choyr Shear Zone, following the granite intrusion at ~136–130 Ma. This time range expresses a ~3–4 Myr crystallization/recrystallization process that overlaps with the one defined by biotite ages between 128.6 ± 0.2 Ma and 125.3 ± 0.3 Ma (Figures 2b, 18, and 21), suggesting temperatures of ~400–450°C [*Villa and Puxeddu*, 1994]. As muscovites exposed to fluids can be affected by recrystallizations under thermal conditions lower than their isotopic closure temperature, as high as 450–500°C [see *Tremblay et al.*, 2011] while biotites are more generally affected by chloritization, the simultaneous end of the muscovite and biotite isotopic record suggests that ductile deformations recorded within the Choyr Shear Zone ended at ~125 Ma (Figure 21).

6.4. Pre-Extension History

[47] In addition to elucidating the structural pattern of the Nartyn area, our geochronological data confirm that country rocks were affected by thermal and tectonic events prior to early Cretaceous extension. Old ages were revealed by $^{40}Ar/^{39}Ar$ spectra obtained from micas collected within the crystalline rocks of the basement (Figure 2b). Two muscovite ages (MN315 and MN319a) suggest that some domains could be older than ~360 Ma (Figure 17g). Similarly, data obtained in the migmatitic xenolith from the Nartyn intrusion from zircons and xenotime cores point to histories older than ~300 Ma (Figures 14c and 14e).

[48] Although most mica sampled close to the Nartyn intrusion yielded early Cretaceous ages that likely date granite emplacement and a subsequent cooling, a muscovite from a slate (MN352a) and two amphiboles from a skarn (MN356a) and from a mafic rock (MN366) yielded middle-late Triassic ages (~235–204 Ma) (Figures 2b, 17e, and 17f). Comparable (re)crystallization ages were also recorded by amphiboles from large amphibolite sheets (MN426a, MN469, MN467, and MN470) (Figures 8a, 16c, 16d, and 16e), as well as monazites from a migmatitic sheet (MN471) (Figure 14d) of the northern part of the Nartyn intrusion. An amphibole from the Choyr Shear Zone (MN401b) yielded a disturbed $^{40}Ar/^{39}Ar$ age spectrum also suggesting some early event prior to ~200 Ma (Figure 18h). All these results indicate that the basement of the Nartyn area was affected by a metamorphic event during late-Triassic time, possibly accompanied by magmatic activity, as suggested by a ~217 Ma muscovite age yielded by a pegmatite dyke (M353a) (Figures 2b and 17e).

7. Geodynamic Implications

7.1. Pre-Extensional Tectonics in Eastern Mongolia

[49] Structural observations indicate that some preserved domains of the basement within the Nartyn area were affected by steeply dipping fabrics probably related to approximately north–south compressive tectonics prior to early Cretaceous extension. This deformation could be related to the final accretion of the Central Asian Orogenic Belt that ended with closure of the Paleo-Asian Ocean and the subsequent Mongolia-North China Craton collision in late Paleozoic or early Mesozoic time [e.g., *Hsü et al.*, 1991; *Şengör and Natal'in*, 1996; *Xiao et al.*, 2003; *Chen et al.*, 2009].

[50] Our geochronological results further indicate that the Nartyn area experienced thermal activity in the middle-late Triassic. These results support previous observations that suggest a period of widespread magmatic activity during the middle-late Triassic in the Central Asian Orogenic Belt [e.g., *Yarmolyuk and Kovalenko*, 2001; *Kovalenko et al.*, 2004; *Jahn et al.*, 2009; *Reichow et al.*, 2010], but also emphasize that high-grade metamorphic conditions prevailed locally during this period.

7.2. Early Cretaceous Extension

[51] Emplacement of the Nartyn and Altanshiree intrusions at ~136–130 Ma and ~134–128 Ma, respectively, appears consistent with a peak of magmatic activity previously documented in northeastern China at ~130–120 Ma [*Wu et al.*, 2005; *Wang et al.*, 2006] and with the occurrence of early Cretaceous plutons in Transbaikalia - northern Mongolia, which continued to ~120 Ma [*Litvinovsky et al.*, 1999, 2002, 2005; *Badanina et al.*, 2006; *Jahn et al.*, 2009; *Zagorsky and Peretyazhko*, 2010].

[52] To our knowledge, only rare studies have documented early Cretaceous syn-extension intrusions in northeastern Asia. The Yagan-Onch Hayrhan metamorphic core complex located at the southern most part of the Chinese-Mongolian border contains syn-kinematic granitoids in its footwall [*Webb et al.*, 1999; *Wang et al.*, 2004]. One was dated by U-Pb on zircons at 135 ± 3 Ma [*Wang et al.*, 2004]. Another study is focused on the Guojianling granodiorite located in the northern part of the Linglong metamorphic core complex on the Jiaodong Peninsula [*Charles et al.*, 2011]. The intrusion dated by SHRIMP U-Pb on zircons to ~130–126 Ma [*Guan et al.*, 1998; *Wang et al.*, 1998], and appears to have been emplaced below a low-angle normal shear zone. However, *Charles et al.* [2011] point out that the intrusion cuts across the northern border of the Linglong core complex, presumably formed in late Jurassic-early Cretaceous times. The timing of exhumation of the Linglong core complex is bracketed by U-Pb zircon dates obtained from high-grade rocks of the dome around 160–150 Ma [*Miao et al.*, 1998; *Wang et al.*, 1998; *Luo et al.*, 1999] and the emplacement age of the Guojianling granodiorite at ~130–126 Ma [*Guan et al.*, 1998; *Wang et al.*, 1998]. *Charles et al.* [2011] proposed that the formation of the Linglong metamorphic core complex in late Jurassic times may have implied a large amount of crustal extension, whereas the emplacement of the

syn-kinematic intrusion in early Cretaceous is associated with more limited of extension.

[53] Our geochronological data indicate that the emplacement of the Nartyn and Altanshiree granites was coeval with that of the Guojianling granodiorite. Northeast of the study areas, the Ereendavaa metamorphic core complex (Figure 1) was exhumed from at least ~138 Ma to 125 Ma [*Daoudene et al.*, 2011]. Although more geochronological data are required to better constrain the timing of exhumation of metamorphic core complexes in Transbaikalia, available ages range from ~133 Ma and ~126 Ma [*Sklyarov et al.*, 1997; *Donskaya et al.*, 2008]. Geochronological data from metamorphic core complexes located in northeastern China consistently suggest exhumation in the ~136–110 Ma time range [*Webb et al.*, 1999; *Davis et al.*, 2002; *Zhang et al.*, 2002, 2003]. Thus, emplacement ages of the Nartyn and Altanshiree intrusions are comparable to those attributed to the exhumation of most metamorphic core complexes from Transbaikalia-northern Mongolia to northeastern China [*Daoudene et al.*, 2011].

[54] *Daoudene et al.* [2011] proposed that an extensional paroxysm at the scale of eastern Asia occurred in a narrow time range in the early Cretaceous, between ~130 Ma and ~120 Ma. However, *Daoudene et al.* [2011] showed that cooling and exhumation of the Ereendavaa metamorphic core complex (Figure 1) might have begun as early as ~138 Ma. This is consistent with the cooling age of 138.2 ± 0.4 Ma obtained on an amphibole collected from the Choyr Shear Zone (Figures 2b and 18e). *Daoudene et al.* [2011] also showed that pegmatite dykes were emplaced ~30 Ma prior to the exhumation history of the Ereendavaa metamorphic core complex. In such a pre-extensional magmatic context, the ~147–149 Ma crystallization ages of monazites from the Nartyn and Altanshiree granites (Figures 2b, 12, 14b, 14h, and 21), as well as the ~146 Ma age of zircons from the Altanshiree granite (Figure 14g), could be related to a stage of partial melting at depth, ~13–19 Myr prior to intrusion emplacements. This hypothesis is in agreement with early fluid-induced crystallization steps at ~150 Ma suspected in the Jirgalanta depression (Figures 2b and 17d). This long-term maturation of the exhumation process appears also consistent with a U-Pb age of 153.9 ± 4.1 obtained on zircons from a migmatite of the Gudaoling metamorphic core complex, north of the Lioaning metamorphic dome on the Liaodong Peninsula [*Charles*, 2010], as well as with the upper-Jurassic ages obtained from high-grade rocks of the Linglong core complex around 160–150 Ma [*Miao et al.*, 1998; *Wang et al.*, 1998; *Luo et al.*, 1999].

[55] In addition with these recent geochronological results, others studies highlight that the eastern part of the Central Asian Orogenic Belt was the locus of widespread magmatic activity starting at 170–160 Ma [*Yarmolyuk et al.*, 1998; *Yarmolyuk and Kovalenko*, 2001; *Kovalenko et al.*, 2004; *Jahn et al.*, 2009] and even slightly earlier [*Wu et al.*, 2003a]. This suggests that the whole region was abnormally hot prior to extension, a feature confirmed by the geochemistry of late Jurassic to early Cretaceous plutons involving mantle-derived sources [e.g., *Wu et al.*, 2003b; *Jahn et al.*, 2009].

8. Conclusions

[56] Structural patterns of the Nartyn and Altanshiree granites show that they emplaced during regional-scale continental extension. U-Pb zircon ages and $^{40}Ar/^{39}Ar$ ages indicate that the Nartyn and Altanshiree granites were emplaced around ~136–130 Ma and 134–128 Ma, respectively. $^{40}Ar/^{39}Ar$ ages also suggest that the Nartyn and Altanshiree granites cooled until at least 129–127 Ma. Emplacement of the Nartyn granite accompanied the development of a low angle normal shear zone, the Choyr Shear Zone, at its northwestern boundary. The evolution of the shear zone lasted at least ~13 Myr, from ~138 Ma to ~125 Ma.

[57] In both studied regions, extensional tectonics involved distributed crustal thinning, with limited exhumation associated with detachment as exemplified in the Nartyn areas. These features differ from classical Metamorphic Core Complexes, where localization of high strain along a low-angle normal shear zone induces a strong exhumation of the ductile middle to lower crust.

[58] Early Cretaceous deformation in the Nartyn and Altanshiree areas resulted from NW-SE directed extension, which is consistent with that documented for neighboring regions from Transbaikalia-northeastern Mongolia to northeastern China. Our geochronological analysis, together with those previously published for other areas of eastern Asia, argues for a paroxysm of extension during lower-Cretaceous times. Our results further confirm that an important thermal-tectonic event occurred in middle-late Triassic times in the region.

[59] **Acknowledgments.** This study was initiated by the Bureau de Recherche Géologique et Minière (BRGM) and was sponsored by the BRGM and the AREVA mining company. It is part of the PhD work of Y. Daoudene that was financially supported by AREVA. Reviews by L. Schoenbohm, L. Webb, and an anonymous reviewer were very constructive.

References

Alexandrov, P., G. Ruffet, and A. Cheilletz (2002), Muscovite recrystallization and saddle-shaped $^{40}Ar/^{39}Ar$ age spectra: Example from the Blond granite (Massif Central, France), *Geochim. Cosmochim. Acta*, *66*, 1793–1807, doi:10.1016/S0016-7037(01)00895-X.

Allen, M. B., D. I. M. McDonald, Z. Xun, S. J. Vincent, and C. Brouet-Menzies (1998), Transtensional deformation in the evolution of the Bohai Basin, northern China, in *Continental Transpressional and Transtensional Tectonics*, edited by R. E. Holdsworth, R. A. Strachan, and J. F. Dewey, *Geol. Soc. Spec. Publ.*, *135*, 215–229.

Amantov, V. A. (1966), First discovery of the lower Cambrian deposits in Eastern Mongolia, in *Materials for Geology of Mongolian People's Republic*, edited by N. A. Marinov, pp. 13–15, Nedra, Moscow.

Badanina, E. V., R. B. Trumbull, P. Dulski, M. Wiedenbeck, I. V. Velksler, and L. F. Syristo (2006), The behavior of rare-earth and lithophile trace elements in rare-metal granites: A study of fluorite, melt inclusions and host rocks from the Khangilay complex, Transbaikalia, Russia, *Can. Mineral.*, *44*, 667–692, doi:10.2113/gscanmin.44.3.667.

Badarch, G., W. D. Cunningham, and B. F. Windley (2002), A new terrane subdivision for Mongolia: Implications for the Phanerozoic crustal growth of Central Asia, *J. Asian Earth Sci.*, *21*, 87–110, doi:10.1016/S1367-9120(02)00017-2.

Blumenfel, P. (1983), Le "tuilage des megacristaux", un critère d'écoulement rotationnel pour les fluidalités des roches magmatiques. Application au granite de Barbey-Séroux (Vosges, France), *Bull. Soc. Geol. Fr.*, *25*, 309–318.

Blumenfeld, P., D. Mainprice, and J. L. Bouchez (1986), C-slip in quartz from subsolidus deformed granite, *Tectonophysics*, *127*, 97–115, doi:10.1016/0040-1951(86)90081-8.

Brun, J. P. (1999), Narrrow rifts versus wide rifts; inference for the mechanics of rifting from laboratory experiments, *Philos. Trans. R. Soc. London A*, *357*, 695–712, doi:10.1098/rsta.1999.0349.

Byamba, J., S. Lkhundev, and S. Tundev (1990), New data on age of Upper Proterozoic deposits in Middle Gobi, *Dokl. Akad. Nauk SSSR*, *312*(12), 428–431.

Cagnard, F., D. Gapais, J. P. Brun, J. Van den Driessche, and C. Gumiaux (2004), Late-Hercynian crustal-scale extension in Vendée (Armorican Massif, France), *J. Struct. Geol.*, *26*(3), 435–449, doi:10.1016/j.jsg.2003.08.006.

Castonguay, S., G. Ruffet, A. Trembay, and G. Féraud (2001), Tectonometamorphic evolution of the southern Quebec Appalachians: $^{40}Ar/^{39}Ar$ evidence for middle Ordovician crustal thickening and Silurian-Early Devonian exhumation of the internal Humber zone, *Geol. Soc. Am. Bull.*, *113*, 144–160, doi:10.1130/0016-7606(2001)113<0144:TEOTSQ>2.0.CO;2.

Castonguay, S., G. Ruffet, and A. Tremblay (2007), Dating polyphase deformation across low-grade metamorphic belts: An example based on $^{40}Ar/^{39}Ar$ muscovite age constraints from the southern Quebec Appalachians, Canada, *Geol. Soc. Am. Bull.*, *119*, 978–992, doi:10.1130/B26046.1.

Charles, N. (2010), Mécanismes de l'extension continentale au Mésozoïque en Asie de l'Est, PhD dissertation, 475 p., Inst. des Sciences de la Terre d'Orléans, Univ. d'Orléans, Orléans, France.

Charles, N., C. Gumiaux, R. Augier, Y. Chen, R. Zhu, and W. Lin (2011), Metamorphic core complexes vs. synkinematic setting: Insights from key structures (Shandong Province, eastern China), *J. Asian Earth Sci.*, *40*(1), 261–278, doi:10.1016/j.jseaes.2010.07.006.

Cheilletz, A., G. Ruffet, C. Marignac, O. Kolli, D. Gasquet, and G. Féraud (1999), $^{40}Ar/^{39}Ar$ dating of shear zones in the Variscan basement of Greater Kabyllia (Algeria). Evidence of an Eo-Alpine event at 128 Ma (Hauterivian-Barremian boundary): Geodynamic consequences, *Tectonophysics*, *306*, 97–116, doi:10.1016/S0040-1951(99)00047-5.

Chen, B., B. M. Jahn, and W. Tian (2009), Evolution of the Solonker suture zone: Constraints from zircon U-Pb ages, Hf isotopic ratios and whole-rock Nd-Sr isotope compositions of subduction- and collision related magmas and forearc sediments, *J. Asian Earth Sci.*, *34*, 245–257, doi:10.1016/j.jseaes.2008.05.007.

Cocherie, A., and O. Legendre (2007), Potential minerals for determining U-Th-Pb chemical age using electron microprobe, *Lithos*, *93*, 288–309, doi:10.1016/j.lithos.2006.03.069.

Daoudene, Y., D. Gapais, P. Ledru, A. Cocherie, S. Hocquet, and T. V. Donskaya (2009), The Ereendavaa Range (north-eastern Mongolia): An additional argument for Mesozoic extension throughout eastern Asia, *Int. J. Earth Sci.*, *98*(6), 1381–1393, doi:10.1007/s00531-008-0412-2.

Daoudene, Y., G. Ruffet, A. Cocherie, P. Ledru, and D. Gapais (2011), Timing of exhumation of the Ereendavaa metamorphic core complex (north-eastern Mongolia)–U-Pb and $^{40}Ar/^{39}Ar$ constraints, *J. Asian Earth Sci.*, doi:10.1016/j.jseaes.2011.04.009, in press.

Darby, B. J., G. A. Davis, X. Zhang, F. Y. Wu, S. A. Wilde, and J. H. Yang (2004), The newly discovered Waziyu metamorphic core complex, Yiwulüshan, western Liaoning province, North China, *Earth Sci. Front*, *11*(3), 145–155.

Davis, G. A., X. L. Qian, Y. D. Zheng, H. Yu, C. Wang, H. M. Tong, C. E. Gehrels, M. Shafiquallah, and J. E. Fryxell (1996), Mesozoic deformation and plutonism in the Yunmeng Shan: A Chinese metamorphic core complex north of Beijing, China, in *The Tectonic Evolution of Asia*, edited by A. Yin and T. M. Harisson, pp. 253–280, Cambridge Univ. Press, Cambridge, U. K.

Davis, G. A., B. J. Darby, Y. Zheng, and T. L. Spell (2002), Geometric and temporal evolution of an extensional detachment fault, Hohhot metamorphic core complex, Inner Mongolia, China, *Geology*, *30*(11), 1003–1006, doi:10.1130/0091-7613(2002)030<1003:GATEOA>2.0.CO;2.

Davis, G. H. (1983), Shear-zone model for the origin of metamorphic core complexes, *Geology*, *11*, 342–347, doi:10.1130/0091-7613(1983)11<342:SMFTOO>2.0.CO;2.

de Jong, K., B. Wang, M. Faure, L. S. Shu, D. Cluzel, J. Charvet, G. Ruffet, and Y. Chen (2009), New $^{40}Ar/^{39}Ar$ age constraints on the Paleozoic tectonic evolution of the western Tianshan (Xinjiang, northwestern China), with emphasis on Permian fluid ingress, *Int. J. Earth Sci.*, *98*, 1239–1258, doi:10.1007/s00531-008-0338-8.

Donskaya, T. V., B. F. Windley, A. M. Mazukabzov, A. Kröner, E. V. Sklyarov, D. P. Gladkochub, V. A. Ponomarchuk, G. Badarch, M. K. Reichow, and E. Hegner (2008), Age and evolution of late Mesozoic metamorphic core complexes in southern Siberia and northern Mongolia, *J. Geol. Soc.*, *165*, 405–421, doi:10.1144/0016-76492006-162.

Erdenetsogt, B. O., I. Lee, D. Bat-Erdene, and L. Jargal (2009), Mongolian coal-bearing basins: Geological settings, coal characteristics, distribution, and resources, *Int. J. Coal Geol.*, *80*, 87–104, doi:10.1016/j.coal.2009.08.002.

Gapais, D., and B. Barbarin (1986), Quartz fabric transition in cooling syntectonic granite (Hermitage massif, France), *Tectonophysics*, *125*, 357–370, doi:10.1016/0040-1951(86)90171-X.

Gow, N. N., and T. C. Pool (2007), Technical report on the uranium exploration properties in Mongolia, prepared for Denison Mines Corp., *Rep. NI 43–101*, Scott Wilson Roscoe Postle Assoc., Toronto, Ont., Canada.

Graham, S. A., M. S. Hendrix, C. L. Johnson, D. Badamgarav, G. Badarch, J. Amory, M. Porter, R. Barsbold, L. E. Webb, and B. R. Hacker (2001), Sedimentary record and tectonic implication of Mesozoic rifting in southeast Mongolia, *Geol. Soc. Am. Bull.*, *113*, 1560–1579, doi:10.1130/0016-7606(2001)113<1560:SRATIO>2.0.CO;2.

Guan, K., Z. Luo, L. Miao, and J. Huang (1998), SHRIMP in zircon chronology for Guojialing suite granite in Jiaodong Zhaoye district [in Chinese with English abstract], *Sci. Geol. Sin.*, *33*, 318–328.

Hanes, J. A., D. York, and C. M. Hall (1985), An $^{40}Ar/^{39}Ar$ geochronological and electron microprobe investigation of an Archean pyroxenite and its bearing on ancient atmospheric compositions, *Can. J. Earth Sci.*, *22*, 947–958, doi:10.1139/e85-100.

Hicks, J. F., D. L. Brinkman, D. J. Nichols, and M. Watabe (1999), Paleomagnetic and palynologic analyses of Albian to Santonian strata at Bayn Shireh, Burkhant, and Khuren Dukh, eastern Gobi Desert, Mongolia, *Cretaceous Res.*, *20*, 829–850, doi:10.1006/cres.1999.0188.

Hsü, K. J., Q. C. Wang, L. Li, and J. Hao (1991), Geological evolution of the Neimonides: Aworking hypothesis, *Eclogae Geol. Helv.*, *84*(1), 1–31.

Ito, M., M. Matsukawa, T. Saito, and D. J. Nichols (2006), Facies architecture and paleohydrology of a synrift succession in the Early Cretaceous Choyr Basin, southeastern Mongolia, *Cretaceous Res.*, *27*, 226–240, doi:10.1016/j.cretres.2005.11.005.

Jahn, B. M., B. A. Litvinosky, A. N. Zanvilevich, and M. Reichow (2009), Peralkaline granitoid magmatism in the Mongolian-Transbaikalian Belt: Evolution petrogenesis and tectonic significance, *Lithos*, *113*, 521–539, doi:10.1016/j.lithos.2009.06.015.

Khain, E. V., E. V. Bibikova, A. Kröner, D. Z. Zhuravlev, E. V. Sklyarov, A. A. Fedotova, and I. R. Kravchenko-Berezhnoy (2002), The most ancient ophiolite of the Central Asian fold belt: U-Pb and Pb-Pb zircon ages for the Dunzhugur Complex, Eastern Sayan, Siberia, and geodynamic implications, *Earth Planet. Sci. Lett.*, *199*, 311–325, doi:10.1016/S0012-821X(02)00587-3.

Khand, Y., D. Badamgarav, Y. Ariunchimeg, and R. Barsbold (2000), Cretaceous system in Mongolia and its depositional environments, in *Cretaceous Environments of Asia*, *Dev. Palaeontol. Stratigr.*, vol. 17, edited by H. Okada and N. J. Mateer, pp. 49–79, Elsevier, Amsterdam, doi:10.1016/S0920-5446(00)80024-2.

Kovalenko, V. I., V. V. Yarmolyuk, V. P. Kovach, A. B. Kotov, I. K. Kozakov, E. B. Salnikova, and A. M. Larin (2004), Isotope province, mechanisms of generation and sources of the continental crust in the Central Asian mobile belt: Geological and isotopic evidence, *J. Asian Earth Sci.*, *23*, 605–627, doi:10.1016/S1367-9120(03)00130-5.

Lin, W., and Q. C. Wang (2006), Late extensional tectonics in the North China block: A crustal response to subcontinental mantle removal?, *Bull. Soc. Geol. Fr.*, *177*, 287–297, doi:10.2113/gssgfbull.177.6.287.

Lin, W., M. Faure, P. Monié, U. Schärer, and D. Panis (2008), Mesozoic extensional tectonics in eastern Asia: The South Liaodong Peninsula metamorphic core complex (NE China), *J. Geol.*, *116*, 134–154, doi:10.1086/527456.

Litvinovsky, B. A., A. N. Zanvilevich, S. M. Wicham, and I. M. Steele (1999), Origin of syenite magmas in A-type granitoid series: Syenite-granite serie from Transbaikalia, *Petrology*, *7*, 483–508.

Litvinovsky, B. A., B. M. Jahn, A. Saunders, S. Poulain, D. V. Kuzmin, M. K. Reichow, and A. V. Tiotov (2002), Petrogenesis of syenite-granite suites from the Bryansky Complex (Transbaikalian, Russia): Implications for the origin of A-type granitoid magmas, *Chem. Geol.*, *189*, 105–133, doi:10.1016/S0009-2541(02)00142-0.

Litvinovsky, B. A., V. V. Yarmolyuk, A. N. Zanvilevich, M. G. Shadaev, A. V. Nikiforov, and V. F. Posokhov (2005), Sources of material and genesis of granite pegmatites of the Oshurkovskii alkaline monzonite massif, Transbaikalia, *Geochem. Int.*, *43*(12), 1149–1167.

Liu, J., G. A. Davis, Z. Lin, and F. Y. Wu (2005), The Liaonan metamorphic core complex, Southeastern Liaoning Province, North China: A likely contributor to Cretaceous rotation of Eastern Liaoning, Korea and contiguous areas, *Tectonophysics*, *407*, 65–80, doi:10.1016/j.tecto.2005.07.001.

Luo, Z., K. Guan, L. Miao, and J. Huang (1999), The ages and its significance of inherited zircons in the granitoid in Zhaoyuan-Laizhou area [in Chinese with English abstract], *Geol. Shandong*, *3*, 24–30.

Mainprice, D., J. L. Bouchez, P. Blumenfeld, and J. M. Tubia (1986), Dominant c-slip in naturally deformed quartz: Implications for dramatic plastic softening at high temperature, *Geology*, *14*, 819–822, doi:10.1130/0091-7613(1986)14<819:DCSIND>2.0.CO;2.

Matsukawa, M., H. Nagata, Y. Taketani, Y. Khanda, P. Khosbajar, D. Badamgarav, and I. Obata (1997), Dinosaur bearing lower Cretaceous

deposits in the Choir Basin, S.E. Mongolia–Stratigraphy and sedimentary environments, *J. Geol. Soc. Philipp.*, *52*, 99–114.

Mazukabzov, A. M., T. V. Donskaya, D. P. Gladkochub, E. V. Sklyarov, V. A. Ponomarchuk, and E. B. Sal'nikova (2006), Structure and age of the metamorphic core complex of the Burgutui ridge (South-western Transbaikalia region), *Dokl. Earth Sci.*, *407*, 179–183, doi:10.1134/S1028334X06020048.

Meng, Q. R. (2003), What drove late Mesozoic extension of the northern China-Mongolia tract?, *Tectonophysics*, *369*, 155–174, doi:10.1016/S0040-1951(03)00195-1.

Meng, Q. R., J. M. Hu, J. Q. Jin, Y. Zhang, and D. F. Xu (2003), Tectonics of the late Mesozoic wide extensional basin system in China-Mongolia border region, *Basin Res.*, *15*, 397–415, doi:10.1046/j.1365-2117.2003.00209.x.

Miao, L., Z. Luo, K. Guan, and J. Huang (1998), The implication of the SHRIMP U-Pb age in zircon to the petrogenesis of the Linglong granite, East Shandong Province [in Chinese with English abstract], *Acta Petrol. Sin.*, *14*, 198–206.

Miller, E. L., P. B. Gans, and J. Garing (1983), The Snake range décollement: An exhumed mid-tertiary ductile-brittle transition, *Tectonics*, *2*(3), 239–263, doi:10.1029/TC002i003p00239.

Mossakovsky, A. A., S. V. Ruzhentsev, S. G. Samygin, and T. N. Kheraskova (1993), Central Asian fold belt: Evolution and formation history, *Geotectonics, Engl. Transl.*, *27*, 445–474.

Nichols, D. J., M. Matsukawa, and M. Ito (2006), Palynology and age of the nonmarine deposits in Mongolia and China, *Cretaceous Res.*, *27*, 241–251, doi:10.1016/j.cretres.2005.11.004.

Paterson, S. R., R. H. Vernon, and O. T. Tobisch (1989), A review of criteria for the identification of magmatic and tectonic foliations in granitoids, *J. Struct. Geol.*, *11*, 349–363, doi:10.1016/0191-8141(89)90074-6.

Pryer, L. L. (1993), Microstructures in feldspars from a major crustal thrust zone: The Grenville Front, Ontario, Canada, *J. Struct. Geol.*, *15*(1), 21–36, doi:10.1016/0191-8141(93)90076-M.

Reichow, M. K., B. A. Litvinovsky, R. R. Parrish, and A. D. Saunders (2010), Multi-stage emplacement of alkaline and peralkaline syenite-granite suites in the Mongolian-Transbaikalian Belt, Russia: Evidence from U-Pb geochronology and whole rock geochemistry, *Chem. Geol.*, *273*, 120–135, doi:10.1016/j.chemgeo.2010.02.017.

Ren, J., K. Tamaki, S. Li, and J. Zhang (2002), Late Mesozoic and Cenozoic rifting an dits dynamic setting in eastern China and adjacent areas, *Tectonophysics*, *344*, 175–205, doi:10.1016/S0040-1951(01)00271-2.

Roddick, J. C., R. A. Cliff, and D. C. Rex (1980), The evolution of excess argon in the Alpine biotites — $^{40}Ar/^{39}Ar$ analysis, *Earth Planet. Sci. Lett.*, *48*, 185–208, doi:10.1016/0012-821X(80)90181-8.

Saiki, K., and A. Okubo (2006), Lower Cretaceous flora of the Choyr Basin, Mongolia, *Cretaceous Res.*, *27*, 252–261, doi:10.1016/j.cretres.2005.11.003.

Schmid, S. M., and M. Casey (1986), Complete fabric analysis of some commonly observed quartz C-axis pattern, in *Mineral and Rock Deformation: Laboratory Studies*, *Geophys. Monogr. Ser.*, vol. 36, edited by B. E. Hobbs and H. C. Heard, pp. 263–286, AGU, Washington, D. C., doi:10.1029/GM036p0263.

Şengör, A. M. C., and B. A. Natal'in (1996), Paleotectonic of Asia: Fragments of a synthesis, in *The Tectonic Evolution of Asia*, edited by A. Yin and T. M. Harrison, pp. 486–640, Cambridge Univ. Press, Cambridge, U. K.

Şengör, A. M. C., B. A. Natal'in, and V. S. Burtman (1993), Evolution of the Alaïd tectonic collage and Palaeozoic crustal growth in Eurasia, *Nature*, *364*, 299–307, doi:10.1038/364299a0.

Sha, J., L. Lin, S. Chen, and M. Matsukawa (2006), Some Lower Cretaceous nonmarine bivalves from fluvio-lacustrine deposits bearing dinosaur fossils in Mongolia and northeast China, *Cretaceous Res.*, *27*, 262–278, doi:10.1016/j.cretres.2005.11.002.

Simpson, C. (1985), Deformation of granite rocks across the brittle-ductile transition, *J. Struct. Geol.*, *7*(5), 503–511, doi:10.1016/0191-8141(85)90023-9.

Simpson, C., and R. P. Wintsch (1989), Evidence for deformation-induced K-feldspar replacement by mirmekite, *J. Metamorph. Geol.*, *7*, 261–275, doi:10.1111/j.1525-1314.1989.tb00588.x.

Sklyarov, E. V., A. M. Mazukabzov, T. V. Donskaya, N. A. Doronina, and A. A. Shafeev (1994), Metamorphic core complexes of the Zagan Range (Transbaikalia), *Dokl. Earth Sci.*, *339*, 83–86.

Sklyarov, E. V., A. M. Mazukabzov, and A. I. Mel'nikov (1997), Metamorphic core complexes of the cordilleran type [in Russian], 184 pp., SPC UIGGM Sib. Branch of the RAS, Novosibirsk, Russia.

Stipp, M., H. Stünitz, R. Heilbronner, and S. M. Schmid (2002), The eastern Tonal fault zone: A "natural laboratory" for crystal plastic deformation of quartz over a temperature range from 250 to 700°C, *J. Struct. Geol.*, *24*, 1861–1884, doi:10.1016/S0191-8141(02)00035-4.

Suess, E. (1908), *The Face of the Earth*, vol. 3, Clarendon Press, Oxford, U. K.

Suzuki, K., and M. Adachi (1991), Precambrian provenance and Silurian metamorphism of the Tsubonsawa paragneiss in the South Kitakami terrane, Northeast Japan, revealed by the chemical Th-U-total Pb isochron ages of monazite, zircon and xenotime, *Geochem. J.*, *25*, 357–376, doi:10.2343/geochemj.25.357.

Tera, F., and G. J. Wasserburg (1972), U-Th-Pb systematics in the Apollo 14 basalts and the problem of initial Pb in lunar rocks, *Earth Planet. Sci. Lett.*, *14*, 281–304, doi:10.1016/0012-821X(72)90128-8.

Tirel, C., J. P. Brun, and E. Burov (2004), Thermomechanical modeling of extensional gneiss domes, in *Gneiss Dome in Orogeny: Boulder, Colorado*, edited by C. Whitney, C. Teyssier, and C. S. Siddoway, *Spec. Pap. Geol. Soc. Am.*, *380*, 67–78.

Traynor, J. J., and C. Sladen (1995), Tectonic and stratigraphic evolution of the Mongolian People's Republic and its influence on hydrocarbon geology and potential, *Mar. Pet. Geol.*, *12*, 35–52, doi:10.1016/0264-8172(95)90386-X.

Tremblay, A., G. Ruffet, and S. Castonguay (2000), Acadian metamorphism in the Dunnage zone of southern Québec, northern Appalachians: $^{40}Ar/^{39}Ar$ evidence for collision diachronism, *Geol. Soc. Am. Bull.*, *112*, 136–146, doi:10.1130/0016-7606(2000)112<136:AMITDZ>2.0.CO;2.

Tremblay, A., G. Ruffet, and J. H. Bédard (2011), Obduction of Tethyan-type ophiolites-A case-study from the Thetford-Mines ophiolitic Complex, Quebec Appalachians, Canada, *Lithos*, *125*, 10–26, doi:10.1016/j.lithos.2011.01.003.

Turner, G. (1971), Argon 40-argon 39 dating: The optimization of irradiation parameters, *Earth Planet. Sci. Lett.*, *10*(2), 227–234, doi:10.1016/0012-821X(71)90010-0.

Villa, I. M., and M. Puxeddu (1994), Geochronology of the Larderello geothermal field: New data and the 'closure temperature' issue, *Contrib. Mineral. Petrol.*, *115*, 415–426, doi:10.1007/BF00320975.

Wang, F., X. H. Zhou, L. C. Zhang, J. F. Ying, Y. T. Zhang, F. Y. Wu, and R. X. Zhu (2006), Late Mesozoic volcanism in the Great Xing'an Range (NE China): Timing and implications for the dynamic setting of NE Asia, *Earth Planet. Sci. Lett.*, *251*, 179–198, doi:10.1016/j.epsl.2006.09.007.

Wang, L. G., Y. M. Qiu, N. J. McNaughton, D. I. Groves, Z. K. Luo, J. Z. Huang, L. C. Miao, and Y. K. Liu (1998), Constraints on crustal evolution and gold metallogeny in the Northwestern Jiaodong Peninsula, China, from SHRIMP U-Pb zircon studies of granitoids, *Ore Geol. Rev.*, *13*, 275–291, doi:10.1016/S0169-1368(97)00022-X.

Wang, T., Y. Zheng, T. Li, and Y. Gao (2004), Mesozoic granitic magmatism in extensional tectonics near the Mongolian border in China and its implications for crustal growth, *J. Asian Earth Sci.*, *23*, 715–729, doi:10.1016/S1367-9120(03)00133-0.

Watson, M. P., A. B. Hayward, D. N. Parkinson, and Z. M. Zhang (1987), Plate tectonic history, basin development and petroleum source rock deposition onshore China, *Mar. Pet. Geol.*, *4*, 205–225, doi:10.1016/0264-8172(87)90045-6.

Webb, L. E., S. A. Graham, C. L. Johnson, G. Badarch, and M. S. Hendrix (1999), Occurrence, age and implications of the Yagan-Onch Hayrhan metamorphic core complex, Southern Mongolia, *Geology*, *27*, 143–146, doi:10.1130/0091-7613(1999)027<0143:OAAIOT>2.3.CO;2.

Wu, F. Y., B. M. Jahn, S. A. Wilde, C. H. Lo, T. F. Yui, Q. Lin, W. C. Ge, and D. Y. Sun (2003a), Highly fractionated I-type granites in NE China (I): Geochronology and petrogenesis, *Lithos*, *66*, 241–273, doi:10.1016/S0024-4937(02)00222-0.

Wu, F. Y., B. M. Jahn, S. A. Wilde, C. H. Lo, T. F. Yui, Q. Lin, W. C. Ge, and D. Y. Sun (2003b), Highly fractionated I-type granites in NE China (II): Isotopic geochemistry and implications for crustal growth in the Phanerozoic, *Lithos*, *67*, 191–204, doi:10.1016/S0024-4937(03)00015-X.

Wu, F. Y., J. Q. Lin, S. A. Wilde, X. O. Zhang, and J. H. Yang (2005), Nature and significance of the early Cretaceous giant igneous event in eastern China, *Earth Planet. Sci. Lett.*, *233*, 103–119, doi:10.1016/j.epsl.2005.02.019.

Xiao, W. J., B. F. Windley, J. Hao, and M. G. Zhai (2003), Accretion leading to collision and the Permian Solonker suture, Inner Mongolia, China: Termination of the Central Asia Orogenic Belt, *Tectonics*, *22*(6), 1069, doi:10.1029/2002TC001484.

Yakubchuk, A., R. Seltmann, V. Shatov, and A. Cole (2001), The Altaids: Tectonic evolution and metallogeny, *Soc. Econ. Geol. Newsl.*, *46*, 6–14.

Yanshin, A. L. (1989), Map of Geologic formations of the Mongolian People's Republic, 2 sheets, scale 1:50 000, Nauka, Moscow.

Yarmolyuk, V. V., and V. I. Kovalenko (2001), The Mesozoic-Cainozoic of Mongolia, in *Tectonics, Magmatis,m and Metallogeny of Mongolia*, edited by A. B. Dergunov, pp. 203–244, Routledge, London.

Yarmolyuk, V. V., V. G. Ivanov, and V. I. Kovalenko (1998), Sources of the intraplate magmatism of Western Tranbaikalia in the late Mesozoic-Cenozoic: Trace element and isotope data, *Petrology*, *6*, 101–124.

Zagorsky, V. E., and I. S. Peretyazhko (2010), First $^{40}Ar/^{39}Ar$ determination on the Malkhan granite-pegmatite system: Geodynamic implications, *Dokl. Earth Sci.*, *430*(2), 172–175, doi:10.1134/S1028334X10020054.

Zhang, X. H., T. Li, Z. Pu, and H. Wang (2002), $^{40}Ar/^{39}Ar$ ages of the Louzidian-Dachengzi ductile shear zone near Chifeng, Inner Mongolia and their tectonic significance, *Chin. Sci. Bull.*, *47*(15), 1292–1297, doi:10.1360/02tb9287.

Zhang, X. H., H. Wang, and Y. J. Ma (2003), $^{40}Ar/^{39}Ar$ Age Constraints on two ductile shear zones, Yanshan Intraplate Orogen, North China Craton, *Int. Geol. Rev.*, *45*, 936–947, doi:10.2747/0020-6814.45.10.936.

Zonenshain, L. P., M. I. Kuzmin, L. M. Natapov, and B. M. Page (Eds.) (1990), *Geology of the USSR: A Plate-Tectonic Synthesis*, *Geodyn. Ser*, vol. 21, 242 pp., AGU, Washington, D. C.

Zorin, Y. A. (1999), Geodynamics of the western part of the Mongol-Okhotsk collisional belt, Trans-Baikal region (Russia) and Mongolia, *Tectonophysics*, *306*, 33–56, doi:10.1016/S0040-1951(99)00042-6.

A. Cocherie and E. Gloaguen, BRGM, 3 Av. Claude-Guillemin, BP 36009, F-45060 Orléans CEDEX 2, France.

Y. Daoudene, D. Gapais, and G. Ruffet, Géosciences Rennes, Université de Rennes 1, F-35042 Rennes, CEDEX, France. (daoudene@gmail.com)

P. Ledru, AREVA, KATCO, 282 Dostyk Ave., BG Mines, Almaty 050000, Kazakhstan.